SMEFT analysis of charged lepton flavor violating *B*-meson decays

Md Isha Ali,[*] Utpal Chattopadhyay,[†] N. Rajeev,[‡] and Joydeep Roy[§]
School of Physical Sciences, Indian Association for the Cultivation of Science, 2A and 2B, Raja SC Mallick Road, Jadavpur, Kolkata 700032, India

(Received 20 December 2023; accepted 24 February 2024; published 16 April 2024)

Charged lepton flavor violation (cLFV) processes, potentially important for various beyond the Standard Model physics scenarios are analyzed in the Standard Model effective field theory framework. We consider the most relevant two-quark–two-lepton $(2q2\ell)$ operators for the leptonic and semileptonic LFV B-decay (LFVBD) processes $B_s \to \mu^+ e^-, B^+ \to K^+\mu^+ e^-, B^0 \to K^{*0}\mu^+ e^-$, and $B_s \to \phi\mu^- e^+$. We analyze the interplay among the Wilson coefficients responsible for these LFVBDs and other cLFV processes, like $\mathrm{CR}(\mu \to e), \ell_i \to \ell_j\gamma, \ell_i \to \ell_j\ell_k\ell_m$, and $Z \to \ell_i\ell_j$, to find the maximal possible LFV effects in B-meson decays. We probe the scale of new physics in relation to the constraints imposed by both classes of the LFV decays while considering both the present bounds and future expectations. In view of proposed experiments at LHCb-II and Belle II to study charged LFV processes, we have also provided the upper limits on the indirect constraints on such LFVBDs. For the processes where the B meson is decaying to $\mu^\pm$ and $e^\mp$, we show that new physics can be constrained by an enhancement of 2–4 orders of magnitude on the current sensitivities of the branching ratios of $B^+ \to K^+\mu^+ e^-, B^0 \to K^{*0}\mu^+ e^-$, and $B_s \to \phi\mu^\pm e^\mp$.

DOI: 10.1103/PhysRevD.109.075028

I. INTRODUCTION

The Standard Model (SM) [1] has been extraordinarily successful in elucidating the fundamental interactions between constituent particles. It has made precise predictions that have been verified by experiments at accelerators such as the CERN large electron positron (LEP) [2], Tevatron [3], and the LHC [4]. The discovery of the Higgs boson at the LHC in 2012 [5] was the last missing piece of the SM puzzle, and it firmly establishes the SM as the appropriate theory for the energy range we have explored. However, SM is still far from becoming a comprehensive account of particle physics [6]. There are several experimental facts and theoretical questions that cannot be addressed by staying within the SM framework. These include the gauge hierarchy problem, the mass of neutrinos, the lack of a particle dark matter candidate, and baryon asymmetry of the Universe, among other significant problems that drive our investigation of physics beyond the SM (BSM) scenarios. Direct and indirect avenues exist for exploring the potential existence of new physics (NP). Direct approaches involve detecting new particles through ongoing and upcoming collider experiments, while indirect probes rely on evidence gathered from various low-energy processes. Among the many potential BSM signals, lepton flavor violation (LFV) stands out as an intriguing and promising candidate for investigating NP scenarios.

The SM assumption of the left-handed neutrinos to be massless renders a lepton family number to be a conserved quantity, but the neutrino oscillation experiments confirmed that the lepton flavor conservation is not a symmetry of nature [7,8]. In the minimum extension of the SM where neutrinos have nonvanishing masses, charged lepton flavor violation (cLFV) is enabled via neutrino oscillation. However, it is heavily suppressed[1] by the Glashow-Iliopoulos-Maiani mechanism, making them unobservable in the current experiments [9,10]. We will briefly review the present experimental status of cLFV processes across various sectors, encompassing lepton decays, boson decays, and hadronic decays.

Before the discovery of neutrino oscillation, cLFV was searched in the decays of atmospheric muons without neutrinos [11]. cLFV in muons is well studied in the decays such as $\mu^+ \to e^+\gamma$, $\mu^+ \to e^+e^-e^+$, and $\mu \to e$ conversion via various nuclei (Au, Al, Ti). MEG [12,13] and PSI [14,15] experiments provide the current limit on

[*]isha.ali080@gmail.com
[†]tpuc@iacs.res.in
[‡]spsrn2733@iacs.res.in
[§]spsjr2729@iacs.res.in

[1]By a factor proportional to $(\Delta m^2/m_W^2)^2 \sim 10^{-50}$, Δm^2 being the squared mass differences of the neutrino mass eigenstates.

$\mu^+ \to e^+\gamma$, with MEG setting an upper limit of 4.2×10^{-13} at 90% confidence level (CL) [12]. This bound is the strongest known in the LFV sector. PSI and upgraded MEG II aim to double the muon measurement rate [13]. The SINDRUM experiment at PSI sets the limit for $\mu^+ \to e^+e^-e^+$ at $< 1.0 \times 10^{-12}$ at 90% CL [14]. Mu3e at PSI targets an upper limit of 10^{-16} by 2030 [16]. Similarly, the best upper bound on neutrinoless $\mu \to e$ conversion using gold targets is 7×10^{-13} by SINDRUM II at PSI [15]. Mu2e at Fermilab projects sensitivity to $\mathcal{O}(10^{-17})$ using aluminum targets [17], while COMET at J-PARC aims for $\mathcal{O}(10^{-15})$ and $\mathcal{O}(10^{-17})$ sensitivities in phases 1 and 2 with the same target [18]. DeeMe at J-PARC projects $\mathcal{O}(10^{-13})$ sensitivity using silicon carbide targets [19]. In the τ sector, constraints on τ-cLFV decays are challenging due to lower production rates and shorter lifetime. Moreover, the constraints from τ-cLFV are not as stringent as those for the case of muons. On the other hand, τ-cLFV decays have the potential for neutrinoless semileptonic decays. B factories, such as *BABAR* [20] and Belle [21], have set upper limits on branching fractions like $\tau^- \to \mu^-\gamma$ and $\tau^- \to e^-\gamma$ [22,23]. Belle II aims for greater sensitivity [24]. In addition, $\tau^- \to \ell^-\ell^+\ell^-$ decays are background-free and attractive for LHC experiments, with the strongest limit from LHCb [25]. Apart from the lepton sector, there are promising LFV searches in the bosonic sector involving Z [26,27] and Higgs bosons [28,29] that require high-energy colliders. μ-cLFV and τ-cLFV indirectly constrain the branching fraction of $Z/H \to \ell\ell'$ decays ($\ell^{(\prime)} \in e, \mu, \tau$) [30].

LFV in B-meson decays complements LFV searches in other sectors and these studies are strongly motivated by dedicated experiments, including LHCb and Belle II. Leptonic B-cLFV searches include decays like $B_s^0 \to e\mu$ and $B_s^0 \to \tau\ell$, where $\ell \in e, \mu$. The LHCb experiment has established the most stringent upper limit on the branching fraction at $\mathcal{B}(B_s^0 \to e^\pm\mu^\mp) < 6.3 \times 10^{-9}$ [31] at 90% CL. Similarly, searching for $B_s^0 \to \tau\ell$ channels presents experimental difficulties due to missing energy from τ decays. Nonetheless, LHCb has achieved the strongest constraints on $B_s^0 \to \tau\ell$ branching fraction to be $<4.2 \times 10^{-5}$ [32] at 95% CL. Semileptonic B-cLFV searches include well-known decays like $B \to K^{(*)}\ell\ell'$, with $\ell \in e, \mu, \tau$. The LHCb Collaboration reported an exclusion limit of $\mathcal{B}(B^+ \to K^+\mu^-e^+) < 7 \times 10^{-9}$ [33] at 90% CL, based on run I data with an integrated luminosity of 3 fb^{-1}. Similar searches were performed for decays $B^0 \to K^{*0}(\to K^+\pi^-)\mu^\pm e^\mp$ and $B_s \to \phi(\to K^+K^-)\mu^\pm e^\mp$ using LHCb data up to 13 TeV, corresponding to a total integrated luminosity of 9 fb^{-1} [34]. The current limits set by LHCb on the branching ratios (BRs) are $\mathcal{B}(B^0 \to K^{*0}\mu^-e^+) < 6.8 \times 10^{-9}$ [34] and $\mathcal{B}(B_s \to \phi\mu^\pm e^\mp) < 10.1 \times 10^{-9}$ [34] at 90% CL. The involvement of τ leptons in the final states of these transitions leads to less stringent constraints due to the challenges posed by missing energy during reconstruction. However, with upgrades planned for LHCb (I and II) [35,36] and the full dataset expected from Belle II [24] by the end of this decade, there is a possibility of improving the upper limits on these processes by up to an order of magnitude. In Table I, we have compiled the current and future prospects for all the LFV processes discussed above. In view of these present and predicted future measurements, in this work, we plan to perform an assessment of the maximal possible LFV effects in B-meson decays in a model-independent way.

In the model-dependent category, various popular models have been used to accommodate cLFV processes. These models include the two Higgs doublet model [53–57], supersymmetric (SUSY) extensions of the SM [58–69], the minimal supersymmetric Standard Model [70], and the seesaw mechanism, which explains neutrino masses and mixing, leading to cLFV processes [9,71–75] or flavor symmetry models [76]. Since the last decade, anomalies in B decays proceeding via $b \to s\ell_i\ell_j$ quark level transition have drawn significant attention due to their association with lepton flavor universality violation (LFUV) based on symmetry arguments as provided in Ref. [77]. Various BSM models, which aim to explain LFUV[2] and also introduce the possibility of LFV in B decays, have been studied extensively [78–83]. In addition, such LFV B decays (LFVBDs) appear in Leptoquark models [84–90], extended gauge sectors [91–94], or SUSY models [95].

To date, searches at the LHC have not yielded any direct evidence of a new particle near the electroweak scale. Strong arguments in support of BSM physics and these null results can become the motivation for considering an effective field theory (EFT) approach [96–99] to estimate the level of unknown physics interactions. In contrast to considering a BSM model that is associated with a top-down approach to an EFT framework, one can adopt a bottom-up approach [98,99], and here this refers to the model-independent investigation within the Standard Model effective field theory (SMEFT) [97–100], where the energy scale Λ of effective interactions can be above the reach of current experiments. In SMEFT one considers higher-dimensional effective local operators out of SM fields only. The operators respect SM gauge invariance, and they are suppressed by appropriate powers of Λ. In regard to LFV processes, SMEFT is shown to be a useful tool for estimating any new physics effect at the scale Λ [101–108]. For B-meson decays in particular, such model-independent approaches have been implemented in a few works; a partial set of references include [109,110].

In this work, we study cLFV decays with more emphasis on the leptonic and semileptonic B decays in the SMEFT formalism consisting of dimension-six (dim-6) operators. We also check for indirect constraints on the important Wilson coefficients (WCs) coming from some LFV

[2]Our analysis, in particular, hardly includes any LFUV studies.

TABLE I. Present upper bounds (with 90% CL, unless otherwise specified) and future expected sensitivities of branching ratios for the set of low-energy cLFV transitions relevant for our analysis. For LFVBDs, the numbers within the parenthesis represent the results obtained with 95% CL.

Observables of cLFV modes	Present bounds		Expected future limits	
$\mathrm{BR}(\mu \to e\gamma)$	4.2×10^{-13}	MEG(2016) [12]	6×10^{-14}	MEG II [13]
$\mathrm{BR}(\mu \to eee)$	1.0×10^{-12}	SINDRUM(1988) [14]	10^{-16}	Mu3e [37]
$\mathrm{CR}(\mu - e, \mathrm{Au})$	7.0×10^{-13}	SINDRUM II(2006) [15]	…	…
$\mathrm{CR}(\mu - e, \mathrm{Al})$	…	…	6×10^{-17}	COMET/Mu2e [17,38]
	…	…	10^{-15} (phase I) & 10^{-17} (phase II)	J-PARK [18]
$\mathrm{BR}(\tau \to e\gamma)$	3.3×10^{-8}	*BABAR* (2010) [22]	3×10^{-9}	Belle II [24]
$\mathrm{BR}(\tau \to eee)$	2.7×10^{-8}	*BABAR* (2010) [39]	5×10^{-10}	Belle [40]
$\mathrm{BR}(\tau \to e\mu\mu)$	2.7×10^{-8}	*BABAR* (2010) [39]	5×10^{-10}	Belle II [24]
$\mathrm{BR}(\tau \to \mu\gamma)$	4.2×10^{-8}	Belle (2021) [23]	10^{-9}	Belle II [24]
$\mathrm{BR}(\tau \to \mu\mu\mu)$	2.1×10^{-8}	*BABAR* (2010) [39]	4×10^{-10}	Belle II [24]
$\mathrm{BR}(\tau \to \mu ee)$	1.8×10^{-8}	*BABAR* (2010) [39]	3×10^{-10}	Belle II [24]
$\mathrm{BR}(\tau \to \pi\mu)$	1.1×10^{-7}	*BABAR* (2006) [41]	5×10^{-10}	Belle II [24]
$\mathrm{BR}(\tau \to \rho\mu)$	1.2×10^{-8}	*BABAR* (2011) [42]	2×10^{-10}	Belle II [24]
$\mathrm{BR}(Z \to \mu e)$	1.7×10^{-6} LEP (95% CL) [43]	7.5×10^{-7} LHC (95% CL) [44]	10^{-8}–10^{-10}	CEPC/FCC-ee [45–48]
$\mathrm{BR}(Z \to \tau e)$	9.8×10^{-6} [43]	5.0×10^{-6} [44,49]	10^{-9}	CEPC/FCC-ee [45–48]
$\mathrm{BR}(Z \to \tau\mu)$	1.2×10^{-5} [50]	6.5×10^{-6} [44,49]	10^{-9}	CEPC/FCC-ee [45–48]
$\mathrm{BR}(B^+ \to K^+\mu^-e^+)$	$7.0(9.5) \times 10^{-9}$	LHCb (2019) [33]	…	…
$\mathrm{BR}(B^+ \to K^+\mu^+e^-)$	$6.4(8.8) \times 10^{-9}$	LHCb (2019) [33]	…	…
$\mathrm{BR}(B^0 \to K^{*0}\mu^+e^-)$	$5.7(6.9) \times 10^{-9}$	LHCb (2022) [34]	…	…
$\mathrm{BR}(B^0 \to K^{*0}\mu^-e^+)$	$6.8(7.9) \times 10^{-9}$	LHCb (2022) [34]	…	…
$\mathrm{BR}(B^0 \to K^{*0}\mu^\pm e^\mp)$	$10.1(11.7) \times 10^{-9}$	LHCb (2022) [34]	…	…
$\mathrm{BR}(B_s^0 \to \phi\mu^\pm e^\mp)$	$16(19.8) \times 10^{-9}$	LHCb (2022) [34]	…	…
$\mathrm{BR}(B^+ \to K^+\mu^-\tau^+)$	0.59×10^{-5}	Belle (2022) [51]	…	…
$\mathrm{BR}(B^+ \to K^+\mu^+\tau^-)$	2.45×10^{-5}	Belle (2022) [51]	3.3×10^{-6}	Belle II [24]
$\mathrm{BR}(B^+ \to K^+\tau^\pm e^\mp)$	1.52×10^{-5}	Belle (2022) [51]	2.1×10^{-6}	Belle II [24]
$\mathrm{BR}(B^0 \to K^{*0}\tau^+\mu^-)$	$1.0(1.2) \times 10^{-5}$	LHCb (2022) [52]	…	…
$\mathrm{BR}(B^0 \to K^{*0}\tau^-\mu^+)$	$8.2(9.8) \times 10^{-6}$	LHCb (2022) [52]	…	…
$\mathrm{BR}(B_s^0 \to \mu^\mp e^\pm)$	$5.4(6.3) \times 10^{-9}$	LHCb (2018) [31]	3×10^{-10}	LHCb-II [35]
$\mathrm{BR}(B^0 \to \mu^\pm e^\mp)$	$1.0(1.3) \times 10^{-9}$	LHCb (2018) [31]	…	…
$\mathrm{BR}(B_s^0 \to \tau^\pm e^\mp)$	7.3×10^{-4} (95%)	LHCb (2019) [32]	…	…
$\mathrm{BR}(B^0 \to \tau^\pm e^\mp)$	2.1×10^{-5} (95%)	LHCb (2019) [32]	…	…
$\mathrm{BR}(B_s^0 \to \tau^\pm \mu^\mp)$	4.2×10^{-5} (95%)	LHCb (2019) [32]	…	…
$\mathrm{BR}(B^0 \to \tau^\pm \mu^\mp)$	1.4×10^{-5} (95%)	LHCb (2019) [32]	1.3×10^{-6}	Belle II [24]

processes other than those involving LFVBDs. The above particularly include limits from decays like Conversion Rate (CR) $\mathrm{CR}(\mu \to e)$, $\ell_i \to \ell_j\gamma$, $\ell_i \to \ell_j\ell_k\ell_m$, and $Z \to \ell_i\ell_j$. We will henceforth collectively refer to these as "other LFV processes." We estimate the effects on the WCs by including both current data as well as future expectations from measurements related to the other LFV processes, along with the same from LFVBDs. Thus, we will also probe the interplay of different LFV bounds between the two sets of decays on the WCs considering the prospective improved limits. We discuss scenarios constructed from different SMEFT coefficients by considering one operator at a time or turning on two operators to have nonvanishing WCs at the scale Λ simultaneously. All other operators vanish at the same scale. As mentioned earlier, at the juncture of not receiving any NP result from the LHC, it is important to rely on indirect constraints from LFVBDs, as well as the same from other LFV decays, and thereby limit the SMEFT operators. We are not aware of a comprehensive and updated analysis in this regard in

relation to the above. This additionally motivates us to include the effects of considering at least two-order more stringent BRs for LFVBDs and explore these in relation to the possible future bounds of the other LFV processes.

The paper is organized as follows: In Sec. II, we give a general description of the SMEFT approach to cLFV, with more emphasis given to leptonic and B cLFV decays. In Sec. III, we write down the most general low-energy effective Hamiltonian relevant for cLFV B decays and the effective Lagrangian for other cLFV decays, including $\mu \to eee$ and $\mathrm{CR}(\mu \to e)$. We also enumerate all the relevant SMEFT operators for current analysis and briefly discuss their correlation through renormalization group evolutions (RGEs). In Sec. IV, we discuss our results by constructing various NP scenarios for different SMEFT operators in 1D and 2D analyses. Finally, we conclude in Sec. V.

II. SMEFT APPROACH TO LEPTON FLAVOR VIOLATION

SMEFT describes new physics effects via higher-dimensional operators, with mass dimension greater than 4 and consisting of SM fields at an energy scale Λ that is above the reach of current experiments. The operators are suppressed by appropriate powers of $\Lambda\,(\gg m_W)$ and corresponding Wilson coefficients parametrize the low-energy behavior of such high-energy theory through the running of RGEs of masses and coupling parameters of the theory. The SMEFT Lagrangian is thus given by [99,100]

$$\mathcal{L}_{\mathrm{SMEFT}} = \mathcal{L}_{\mathrm{SM}} + \frac{1}{\Lambda} C^{(5)} \mathcal{O}^{(5)} + \frac{1}{\Lambda^2} \sum_n C_n^{(6)} \mathcal{O}_n^{(6)} + \mathcal{O}\left(\frac{1}{\Lambda^3}\right) + \cdots, \tag{1}$$

where $\mathcal{L}_{\mathrm{SM}}$ is the usual renormalizable SM Lagrangian, $\mathcal{O}^{(5)}$ represents the gauge-invariant mass dimension-five operators, known as the neutrino mass generating Weinberg operator, and $C^{(5)}$ is the corresponding WCs. Similarly, $\mathcal{O}_n^{(6)}$ and $C_n^{(6)}$ represent mass dimension-six operators and corresponding WCs, respectively. In this work, we will adopt the conventions of the Warsaw basis [100] and will not consider any more terms with suppression level greater than $1/\Lambda^2$.

It is known that flavor-changing neutral current (FCNC) processes can be substantially large in many BSM scenarios, whereas they are heavily suppressed in the SM by small Cabibbo-Kobayashi-Maskawa (CKM) matrix elements, loop effects, etc. Probing NP models with FCNC effects can thus be quite useful. Therefore, studying flavor observables in the SMEFT approach, which can provide sensitive NP contributions, has been quite popular. For example, SMEFT has been used to study general LFV processes [102,111,112], B-meson LFV decays [92,93,110,113,114], Z boson LFV decays [115], Higgs boson LFV decays [116], or quarkonium LFV decays [117]. Although these references are hardly an exhaustive list of such works, it has been shown in all of them that most dominant contributions to LFV processes come from dimension-six operators and, furthermore, the operators contributing to semileptonic processes are either of the Higgs-fermion or four-fermion type. With our focus on LFV B-meson decays only, we will not consider the former type in our analysis. A complete list of dimension-six operators is provided in Table II with the boldfaced ones contributing directly to LFVBDs.

TABLE II. A comprehensive list of dimension-six operators that remain invariant under the SM gauge group and contribute to LFV observables. The boldfaced ones are mainly responsible for generating LFVBDs at the tree level. In these expressions, Q and L represent left-handed quark and lepton $SU(2)$ doublets, respectively, with indices a, $b = 1, 2$. U, D, and E denote right-handed up and down quark and lepton singlets, with Φ representing the Higgs doublet [and $\varphi^\dagger \overleftrightarrow{D}_\mu \varphi \equiv \Phi^\dagger (D_\mu \Phi) - (D_\mu \Phi)^\dagger \Phi$]. $B_{\mu\nu}$ and $W^I_{\mu\nu}$ stand for the $U(1)$ and $SU(2)$ field strengths, respectively, while τ^I with $I = 1, 2, 3$ denotes the Pauli matrices. For brevity, flavor indices are not explicitly shown in this list.

Four-lepton operators		Two-lepton–two quark operators	
$\mathcal{O}_{\ell\ell}$	$(\bar{L}\gamma_\mu L)(\bar{L}\gamma^\mu L)$	$\boldsymbol{\mathcal{O}^{(1)}_{\ell q}}$	$\boldsymbol{(\bar{L}\gamma_\mu L)(\bar{Q}\gamma^\mu Q)}$
$\mathcal{O}_{ee}$	$(\bar{E}\gamma_\mu E)(\bar{E}\gamma^\mu E)$	$\boldsymbol{\mathcal{O}^{(3)}_{\ell q}}$	$\boldsymbol{(\bar{L}\gamma_\mu \tau^I L)(\bar{Q}\gamma^\mu \tau^I Q)}$
$\mathcal{O}_{\ell e}$	$(\bar{L}\gamma_\mu L)(\bar{E}\gamma^\mu E)$	$\boldsymbol{\mathcal{O}_{qe}}$	$\boldsymbol{(\bar{Q}\gamma_\mu Q)(\bar{E}\gamma^\mu E)}$
Lepton-Higgs operators		$\boldsymbol{\mathcal{O}_{\ell d}}$	$\boldsymbol{(\bar{L}\gamma_\mu L)(\bar{D}\gamma^\mu D)}$
$\mathcal{O}^{(1)}_{\varphi\ell}$	$i(\varphi^\dagger \overleftrightarrow{D}_\mu \varphi)(\bar{L}\gamma^\mu L)$	$\boldsymbol{\mathcal{O}_{ed}}$	$\boldsymbol{(\bar{E}\gamma_\mu E)(\bar{D}\gamma^\mu D)}$
$\mathcal{O}^{(3)}_{\varphi\ell}$	$i(\varphi^\dagger \overleftrightarrow{D}^I_\mu \varphi)(\bar{L}\tau^I\gamma^\mu L)$	$\boldsymbol{\mathcal{O}_{\ell edq}}$	$\boldsymbol{(\bar{L}^a E)(\bar{D}Q^a)}$
$\mathcal{O}_{\varphi e}$	$i(\varphi^\dagger \overleftrightarrow{D}_\mu \varphi)(\bar{E}\gamma^\mu E)$	$\mathcal{O}^{(1)}_{\ell equ}$	$(\bar{L}^a E)\epsilon_{ab}(\bar{Q}^b U)$
$\mathcal{O}_{e\varphi}$	$(\bar{L}E\Phi)(\Phi^\dagger\Phi)$	$\mathcal{O}^{(3)}_{\ell equ}$	$(\bar{L}^a \sigma_{\mu\nu} E)\epsilon_{ab}(\bar{Q}^b \sigma^{\mu\nu} U)$
Dipole operators		$\mathcal{O}_{\ell u}$	$(\bar{L}\gamma_\mu L)(\bar{U}\gamma^\mu U)$
$\mathcal{O}_{eW}$	$(\bar{L}\sigma^{\mu\nu}E)\tau^I \Phi W^I_{\mu\nu}$	$\mathcal{O}_{eu}$	$(\bar{E}\gamma_\mu E)(\bar{U}\gamma^\mu U)$
$\mathcal{O}_{eB}$	$(\bar{L}\sigma^{\mu\nu}E)\Phi B_{\mu\nu}$		

In general studies of low-energy observables in SMEFT, there are three energy scales. A high-energy scale Λ, an intermediate energy scale of electroweak symmetry-breaking m_W, and a low-energy scale like $\sim m_b$ or $m_{\tau/\mu}$. Therefore, for probing the level of contributions of the higher-dimensional operators for LFV studies that may be consistent with experimental constraints, a general method of "match and run" of RGEs is described below. At the first step, the SMEFT one-loop RGEs [118–120] of relevant WCs would be initialized at the scale $\Lambda(\sim\mathrm{TeV})$ and run down to the electroweak scale $\sim m_{Z,W}$. The WCs under study are given a nonvanishing value like unity, while other WCs are set to zero at the scale Λ and RGE is completed until the electroweak scale m_W. Of course, the WCs are hardly expected to remain at their initial values, including also the ones that were vanishing at the higher scale.

This level of evolutions is adequate for the LFV decays of the Z or Higgs bosons, but not enough for processes referring to energies below the electroweak scale. Further down the scale, in the second step, as in a top-down approach of EFT, the heavy particles of the theory ($W^{\pm}$, Z, the Higgs boson, and the top quark) are integrated out and the operators invariant under the QCD × QED gauge groups and consisting of fields of light charged fermions $(u, d, c, s, b, e, \mu, \tau)$, neutral fermions $(\nu_e, \nu_\mu, \nu_\tau)$, and gauge bosons $(F_{\mu\nu}, G^a_{\mu\nu})$ describe the effective interactions. These operators are known as low-energy effective field theory (LEFT) operators that contribute to the total LEFT Lagrangian containing dimension-three and higher-dimensional ($d > 4$) operators. The most relevant LEFT operators for our purpose are dimension-six operators containing four fermions with at least one spinor combination consisting of two different charged lepton flavors [121]. Schematically, these operators take the form

$$\mathcal{O}_{SAB} = (\bar{\ell}_i \Gamma_S P_A \ell_j)(\bar{f}_\alpha \Gamma_S P_B f_\beta), \tag{2}$$

where $\ell_{i,j}$ are the lepton pairs, $f_{\alpha,\beta}$ are the fermion pairs, $P_{A,B}$ are the left and right projection operators, and $\Gamma_S = \mathbf{1}, \gamma_\mu$, and $\sigma_{\mu\nu}$ for scalar, vector, and tensor, respectively. Following the match and run procedure, one-loop RGEs of these LEFT operators are matched at tree level to the SMEFT operators, the details of which can be found in Refs. [122,123]. In the third and final step of the process, the running of these LEFT operators to the low-energy scale of m_τ, m_μ, or m_b is performed to evaluate the desired experimental observables. We implement all these procedures in our numerical analysis with the help of the WILSON [124] and FLAVIO [125] packages.

III. LOW-ENERGY EFFECTIVE HAMILTONIAN AND BRANCHING RATIOS FOR LFV DECAYS

Keeping the prime focus on the lepton flavor violating B-meson decays, in this section, we shall discuss the effective Hamiltonian or Lagrangians for LFV processes such as $b \to s\ell_i\ell_j$, $\mathrm{CR}(\mu \to e)$, and $\ell_i \to \ell_j\ell_k\bar{\ell}_m$ that are relevant to our analysis. We shall also provide the expression for branching ratios of corresponding processes and that will be followed by the classification of higher-dimensional operators responsible for such processes. Being a relatively less important process for our analysis, the details of Z LFV are given in the Appendix.

A. Lepton flavor violating $b \to s\ell_i\ell_j$ decays

The most general effective Hamiltonian for the weak decay process of a bottom (b) quark to strange (s) quark transition along with two leptons $(\ell_{i,j})$, $b \to s\ell_i\ell_j$, in terms of low-energy dim-6 operators $(\mathcal{O}_n)$ and corresponding Wilson coefficients (C_n) is given by [114,126]

$$\mathcal{H}^{\Delta B=1}_{\mathrm{eff}} = -\frac{4G_F}{\sqrt{2}} V_{tb} V^*_{ts} \left[\sum_{n=7}^{10} C_n(\mu)\mathcal{O}_n(\mu) + C'_n(\mu)\mathcal{O}'_n(\mu) \right], \tag{3}$$

where G_F is the Fermi coupling constant, characterizing the strength of weak interactions, and V_{tb}, V^*_{ts} are the CKM matrix elements. Both $\mathcal{O}^{(\prime)}_n$ and $\mathcal{O}^{(\prime)}_n$ are the functions of the renormalizable energy scale μ, which for our low-energy processes would be taken as the mass of the b quark (m_b). The primed operators are obtained by flipping the chirality, and they are usually highly suppressed compared to their unprimed counterparts in the SM. In Eq. (3), $n = 7$, 8 represent the photon and gluon "magnetic-penguin" operators, whereas $n = 9$, 10 refer to the "semileptonic" operators. They are defined as [114,126]

$$\mathcal{O}_7 = \frac{e}{16\pi^2}\bar{m}_b[\bar{s}_{Li}\sigma^{\mu\nu}b_{Ri}]F_{\mu\nu},$$
$$\mathcal{O}_8 = \frac{g_s}{16\pi^2}\bar{m}_b[\bar{s}_{Li}\sigma^{\mu\nu}T^a_{ij}b_{Ri}]G^a_{\mu\nu}, \tag{4}$$

$$\mathcal{O}_9 = \frac{e^2}{16\pi^2}[\bar{s}_L\gamma_\mu b_L][\overline{\ell}_i\gamma^\mu\ell_j],$$
$$\mathcal{O}_{10} = \frac{e^2}{16\pi^2}[\bar{s}_L\gamma_\mu b_L][\overline{\ell}_i\gamma^\mu\gamma_5\ell_j], \tag{5}$$

where $\ell_{i,j} = e$, μ, τ, respectively. $F_{\mu\nu}$ and $G^a_{\mu\nu}$ are the photon and gluon field strength tensor, respectively, and R, L denote the right- and left-handed projection operators, $P_{R,L} = (1 \pm \gamma_5)/2$. In Eq. (4), g_s is the strong coupling constant, $\bar{m}_b$ denotes the running of b quark mass in the minimal subtraction $(\overline{\mathrm{MS}})$ scheme, and T^a_{ij} represents the color charges. $\mathcal{O}_7$, $\mathcal{O}_8$, $\mathcal{O}_9$, and $\mathcal{O}_{10}$ also have their chiral counterparts, whose explicit structures are given by

$$\mathcal{O}'_7 = \frac{e}{16\pi^2}\bar{m}_b[\bar{s}_{Ri}\sigma^{\mu\nu}b_{Li}]F_{\mu\nu},$$
$$\mathcal{O}'_8 = \frac{g_s}{16\pi^2}\bar{m}_b[\bar{s}_{Ri}\sigma^{\mu\nu}T^a_{ij}b_{Li}]G^a_{\mu\nu}, \tag{6}$$

$$\mathcal{O}'_9 = \frac{e^2}{16\pi^2}[\bar{s}_R\gamma_\mu b_R][\overline{\ell}_i\gamma^\mu\ell_j],$$
$$\mathcal{O}'_{10} = \frac{e^2}{16\pi^2}[\bar{s}_R\gamma_\mu b_R][\overline{\ell}_i\gamma^\mu\gamma_5\ell_j]. \tag{7}$$

In addition to these operators, two scalar, two pseudoscalar, and two tensor NP operators can potentially contribute to B-meson decays [114,127],[3]

$$\mathcal{O}_S = [\bar{s}_L b_R][\overline{\ell}_i\ell_j], \qquad \mathcal{O}'_S = [\bar{s}_R b_L][\overline{\ell}_i\ell_j], \tag{8}$$

[3]It is shown in [113] that the contribution of tensor operators to such decays can be neglected because of not satisfying their noninvariant character under $SU(2)_L \times U(1)_Y$ symmetry.

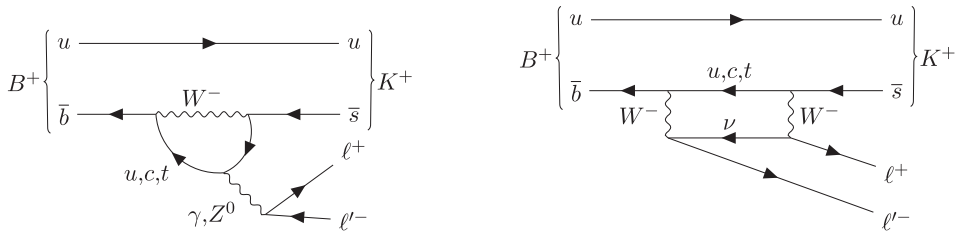

FIG. 1. Feynman diagrams for $B^+ \to K^+\ell^+\ell'^-$. Replacing u quark by d quark leads to similar diagrams for $B^0 \to K^{*0}\ell^+\ell'^-$.

$$\mathcal{O}_P = [\bar{s}_L b_R][\overline{\ell}_i \gamma_5 \ell_j], \qquad \mathcal{O}'_P = [\bar{s}_R b_L][\overline{\ell}_i \gamma_5 \ell_j], \quad (9)$$

$$\mathcal{O}_T = [\bar{s}\sigma_{\mu\nu} b][\overline{\ell}_i \sigma^{\mu\nu} \ell_j], \quad \mathcal{O}_{T5} = [\bar{s}\sigma_{\mu\nu} b][\overline{\ell}_i \sigma^{\mu\nu} \gamma_5 \ell_j]. \quad (10)$$

Generally, $b \to s$ transitions, of which the above-mentioned process is an example, lead to FCNC, which are described in the SM by one-loop diagrams as shown in Fig. 1.

After decomposing the hadronic matrix elements for $B_s \to \ell_i^- \ell_j^+$ decay mode into $\langle 0|\bar{b}\gamma^\mu\gamma_5 s|B_s(p)\rangle = i f_{B_s} p_\mu$, where f_{B_s} is the B_s-meson decay constant, one can obtain the branching fraction containing both vector and scalar kinds of operators as [93]

$$\begin{aligned}\mathrm{Br}[B_s \to \ell_i^- \ell_j^+] = {} & \frac{\tau_{B_s}}{64\pi^3}\frac{\alpha^2 G_F^2}{m_{B_s}^3} f_{B_s}^2 |V_{tb}V_{ts}^*|^2 \lambda^{1/2}(m_{B_s}, m_i, m_j) \\ & \times \left\{ [m_{B_s}^2 - (m_i+m_j)^2] \cdot \left| (C_9^{\ell_i\ell_j} - C_9^{\prime\ell_i\ell_j})(m_i - m_j) + (C_S^{\ell_i\ell_j} - C_S^{\prime\ell_i\ell_j}) \frac{m_{B_s}^2}{m_b + m_s} \right|^2 \right. \\ & \left. + [m_{B_s}^2 - (m_i-m_j)^2] \cdot \left| (C_{10}^{\ell_i\ell_j} - C_{10}^{\prime\ell_i\ell_j})(m_i + m_j) + (C_P^{\ell_i\ell_j} - C_P^{\prime\ell_i\ell_j}) \frac{m_{B_s}^2}{m_b + m_s} \right|^2 \right\}. \end{aligned} \quad (11)$$

For $B \to K^{(*)}\ell_i^+\ell_j^-$, the branching fraction containing both vector and scalar kinds of operators is written as

$$\begin{aligned}\mathrm{Br}[B \to K^{(*)}\ell_i^+\ell_j^-] = 10^{-9}\Big\{ & a_{K^{(*)}\ell_i\ell_j}\left|C_9^{\ell_i\ell_j} + C_9^{\prime\ell_i\ell_j}\right|^2 + b_{K^{(*)}\ell_i\ell_j}\left|C_{10}^{\ell_i\ell_j} + C_{10}^{\prime\ell_i\ell_j}\right|^2 \\ & + c_{K^*\ell_i\ell_j}\left|C_9^{\ell_i\ell_j} - C_9^{\prime\ell_i\ell_j}\right|^2 + d_{K^*\ell_i\ell_j}\left|C_{10}^{\ell_i\ell_j} - C_{10}^{\prime\ell_i\ell_j}\right|^2 \\ & + e_{K^{(*)}\ell_i\ell_j}\left|C_S^{\ell_i\ell_j} + C_S^{\prime\ell_i\ell_j}\right|^2 + f_{K^{(*)}\ell_i\ell_j}\left|C_P^{\ell_i\ell_j} + C_P^{\prime\ell_i\ell_j}\right|^2 \\ & + g_{K^{(*)}\ell_i\ell_j}\left|C_S^{\ell_i\ell_j} - C_S^{\prime\ell_i\ell_j}\right|^2 + h_{K^{(*)}\ell_i\ell_j}\left|C_P^{\ell_i\ell_j} - C_P^{\prime\ell_i\ell_j}\right|^2 \Big\}. \end{aligned} \quad (12)$$

In Eq. (11), τ_{B_s} and M_{B_s} represent the lifetime and mass of the B_s particle, respectively, m_ℓ's are lepton masses, α is the fine-structure constant, and $\lambda(a,b,c) = [a^2 - (b-c)^2][a^2 - (b+c)^2]$. In Eq. (12), $a_{K^{(*)}\ell_i\ell_j} \cdots h_{K^{(*)}\ell_i\ell_j}$ represent numerical values multiplying the WCs are different for a different choice of flavors [93,109]. The experimental data on such LFV processes in B-meson decays are provided by different experimental collaborations as shown in Table I.

When the heavy fields are integrated out from the SMEFT, equating the Hamiltonian (3) at m_W scale with the four-fermion currents that are listed in Table II and keeping the relevant operators only, we get [113]

$$C_9^{\ell_i\ell_j} = \frac{(4\pi)^2}{e^2\lambda_{bs}}\frac{v^2}{\Lambda^2}\left(C_{qe}^{\ell_i\ell_j} + C_{\ell q}^{(1)\ell_i\ell_j} + C_{\ell q}^{(3)\ell_i\ell_j}\right), \quad (13)$$

$$C_9^{\prime\ell_i\ell_j} = \frac{(4\pi)^2}{e^2\lambda_{bs}}\frac{v^2}{\Lambda^2}\left(C_{ed}^{\ell_i\ell_j} + C_{\ell d}^{\ell_i\ell_j}\right), \quad (14)$$

$$C_{10}^{\ell_i\ell_j} = \frac{(4\pi)^2}{e^2\lambda_{bs}}\frac{v^2}{\Lambda^2}\left(C_{qe}^{\ell_i\ell_j} - C_{\ell q}^{(1)\ell_i\ell_j} - C_{\ell q}^{(3)\ell_i\ell_j}\right), \quad (15)$$

$$C_{10}^{\prime\ell_i\ell_j} = \frac{(4\pi)^2}{e^2\lambda_{bs}}\frac{v^2}{\Lambda^2}\left(C_{ed}^{\ell_i\ell_j} - C_{\ell d}^{\ell_i\ell_j}\right) \quad (16)$$

and similarly for scalar and pseudoscalar operators,

$$C_S^{\ell_i\ell_j} = -C_P^{\ell_i\ell_j} = \frac{(4\pi)^2}{e^2\lambda_{bs}}\frac{v^2}{\Lambda^2}C_{\ell edq}^{\ell_i\ell_j}, \tag{17}$$

$$C_S^{\prime\ell_i\ell_j} = C_P^{\prime\ell_i\ell_j} = \frac{(4\pi)^2}{e^2\lambda_{bs}}\frac{v^2}{\Lambda^2}C_{\ell edq}^{\prime\ell_i\ell_j}, \tag{18}$$

where the primed operator $C_{\ell edq}^{\prime\ell_i\ell_j}$ represents a different flavor entry of the Hermitian conjugate of the corresponding unprimed operator, $\lambda_{bs} = V_{tb}V_{ts}^*$.

Looking at the structure of the operators $\mathcal{O}_9^{(\prime)}$, $\mathcal{O}_{10}^{(\prime)}$, $\mathcal{O}_S^{(\prime)}$, and $\mathcal{O}_P^{(\prime)}$ we find that the $2q2\ell$ operators listed in Table II are most relevant for our purpose, as we have already mentioned above. The associated WCs of all these operators are to be evaluated at the b-quark mass scale ($\mu = m_b$) as we are interested in LFV processes in B-meson decays. Therefore, the RGEs of those WCs are needed to run down from some high-energy scale and, as we have mentioned before, such SMEFT running will induce several other WCs that are not explicitly related to LFVBDs. In the following sections, we shall list all dim-6 SMEFT operators contributing to the processes under our consideration.

B. Muon to electron conversion in nuclei [CR($\mu \to e$)]

The most general LFV interaction Lagrangian, which contributes to the $\mu - e$ transition in nuclei, is given by [128]

$$\begin{aligned}\mathcal{L}_{\text{eff}} = &-\frac{4G_{\text{F}}}{\sqrt{2}}(m_\mu A_R\bar{\mu}\sigma^{\mu\nu}P_L eF_{\mu\nu} + m_\mu A_L\bar{\mu}\sigma^{\mu\nu}P_R eF_{\mu\nu} + \text{H.c.}) - \frac{G_{\text{F}}}{\sqrt{2}}\sum_{q=u,d,s}\Big[\Big(g_{LS}^{(q)}\bar{e}P_R\mu + g_{RS}^{(q)}\bar{e}P_L\mu\Big)\bar{q}q \\ &+ \Big(g_{LP}^{(q)}\bar{e}P_R\mu + g_{RP}^{(q)}\bar{e}P_L\mu\Big)\bar{q}\gamma_5 q + \Big(g_{LV}^{(q)}\bar{e}\gamma^\mu P_L\mu + g_{RV}^{(q)}\bar{e}\gamma^\mu P_R\mu\Big)\bar{q}\gamma_\mu q \\ &+ \Big(g_{LA}^{(q)}\bar{e}\gamma^\mu P_L\mu + g_{RA}^{(q)}\bar{e}\gamma^\mu P_R\mu\Big)\bar{q}\gamma_\mu\gamma_5 q + \frac{1}{2}\Big(g_{LT}^{(q)}\bar{e}\sigma^{\mu\nu}P_R\mu + g_{RT}^{(q)}\bar{e}\sigma^{\mu\nu}P_L\mu\Big)\bar{q}\sigma_{\mu\nu}q + \text{H.c.}\Big],\end{aligned} \tag{19}$$

where $A_{L,R}$ and g's are all dimensionless coupling constants for the corresponding operators. From this effective Lagrangian, the μ-e conversion rate in nuclei can be expressed by the formula [129]

$$\Gamma_{\mu\to e\,\text{conv}} = \frac{m_\mu^5}{\omega_{\text{capt}}\Lambda^4}\left\{\left|\tilde{C}_{DL}D + \tilde{C}_{SL}^{(p)}S^{(p)} + \tilde{C}_{SL}^{(n)}S^{(n)} + \tilde{C}_{VL}^{(p)}V^{(p)} + \tilde{C}_{VL}^{(n)}V^{(n)}\right|^2 + |L \leftrightarrow R|^2\right\}, \tag{20}$$

where ω_{capt} is the muon capture rate in nuclei N and $D, S^{(p/n)}$, $V^{(p/n)}$ represent dimensionless overlap integrals for dipole, scalar, and vector operators, respectively. Their numerical values depend on the nuclei and can be found in Ref. [129]. After tree-level matching [122], we obtain that the dipole form factors are given by

$$A_L = \frac{v}{2\sqrt{2}m_\mu}C_\gamma^{e\mu}, \qquad A_R = \frac{v}{2\sqrt{2}m_\mu}C_\gamma^{\mu e*}, \tag{21}$$

the vector form factors by

$$\begin{aligned}\tilde{C}_{VL}^{(p)} &= 2g_{LV,RV}^{(u)} + g_{LV,RV}^{(d)}, \\ \tilde{C}_{VL}^{(n)} &= g_{LV,RV}^{(u)} + 2g_{LV,RV}^{(d)},\end{aligned} \tag{22}$$

with

$$\begin{aligned}g_{VL}^{(u)} = &\left(C_{\ell q}^{(1)} - C_{\ell q}^{(3)} + C_{\ell u}\right)^{e\mu uu} \\ &+ \left(1 - \frac{8}{3}s_{\text{w}}^2\right)\left(C_{\varphi l}^{(1)} + C_{\varphi l}^{(3)}\right)^{e\mu},\end{aligned} \tag{23}$$

$$\begin{aligned}g_{VL}^{(d)} = &\left(C_{\ell q}^{(1)} + C_{\ell q}^{(3)} + C_{\ell d}\right)^{e\mu dd} \\ &- \left(1 - \frac{4}{3}s_{\text{w}}^2\right)\left(C_{\varphi l}^{(1)} + C_{\varphi l}^{(3)}\right)^{e\mu},\end{aligned} \tag{24}$$

$$g_{VR}^{(u)} = C_{eu}^{e\mu uu} + C_{qe}^{uue\mu} + \left(1 - \frac{8}{3}s_{\text{w}}^2\right)C_{\varphi e}^{e\mu}, \tag{25}$$

$$g_{VR}^{(d)} = C_{ed}^{e\mu dd} + C_{qe}^{dde\mu} - \left(1 - \frac{4}{3}s_{\text{w}}^2\right)C_{\varphi e}^{e\mu}, \tag{26}$$

and finally, the scalar form factors by

$$\begin{aligned}\tilde{C}_{SL}^{(p/n)} = &-G_S^{(u,p/n)}C_{\ell equ}^{(1)e\mu uu} + G_S^{(d,p/n)}C_{\ell edq}^{e\mu dd} \\ &+ G_S^{(s,p/n)}C_{\ell edq}^{e\mu ss},\end{aligned} \tag{27}$$

$$\begin{aligned}\tilde{C}_{SR}^{(p/n)} = &-G_S^{(u,p/n)}C_{\ell equ}^{(1)\mu euu*} + G_S^{(d,p/n)}C_{\ell edq}^{\mu edd*} \\ &+ G_S^{(s,p/n)}C_{\ell edq}^{\mu ess*},\end{aligned} \tag{28}$$

with the numerical coefficients [129]

$$G_S^{(u,p)} = G_S^{(d,n)} = 5.1, \qquad G_S^{(u,n)} = G_S^{(d,p)} = 4.3, \qquad G_S^{(s,p)} = G_S^{(s,n)} = 2.5. \tag{29}$$

C. Lepton flavor violating three-body leptonic decays ($\ell_i \to \ell_j \ell_k \overline{\ell}_m$)

Starting from the LEFT Lagrangian [122], the relevant terms for the tree-level three-body decays are

$$\begin{aligned}\mathcal{L}_{\text{LEFT}} \supset\ & C_{ee}^{VLL}(\bar{e}_j\gamma^\mu P_L e_i)(\bar{e}_k\gamma_\mu P_L e_m) + C_{ee}^{VRR}(\bar{e}_j\gamma^\mu P_R e_i)(\bar{e}_k\gamma_\mu P_R e_m) + C_{ee}^{VLR}(\bar{e}_j\gamma^\mu P_L e_i)(\bar{e}_k\gamma_\mu P_R e_m) \\ & + \left\{C_{ee}^{SRR}(\bar{e}_j P_R e_i)(\bar{e}_k P_R e_m) + \text{H.c.}\right\} + \left\{C_\gamma(\bar{e}_j\sigma^{\mu\nu} P_R e_i)F_{\mu\nu} + \text{H.c.}\right\}.\end{aligned} \tag{30}$$

The expressions for the decays depend on the flavor combinations of the final leptons, as they could involve new possible contractions and symmetry factors. Therefore, the general expression for the branching ratio of three-body charged lepton decays is given by [111]

$$\begin{aligned}\text{Br}(\ell_i \to \ell_j \ell_k \overline{\ell}_l) = \frac{N_c M^5}{6144\pi^3\Lambda^4\Gamma_{\ell_i}}&(4(|C_{VLL}|^2 + |C_{VRR}|^2 + |C_{VLR}|^2 + |C_{VRL}|^2) + |C_{SLL}|^2 \\ & + |C_{SRR}|^2 + |C_{SLR}|^2 + |C_{SRL}|^2 48(|C_{TL}|^2 + |C_{TR}|^2) + X_\gamma),\end{aligned} \tag{31}$$

where $N_c = 1/2$ if two of the final state leptons are identical, $N_c = 1$ in all other cases, and Γ_{ℓ_i} is the total decay width of the initial lepton. Because of the hierarchy of the charged lepton masses, it is assumed that $m_i \equiv M \gg m_j, m_k, m_l$ and the lighter lepton masses are neglected. C_X are different for different processes. For decay of the type $\ell_i \to \ell_j \ell_j \overline{\ell}_j$,

$$C_{VLL} = 2\left((2s_W^2 - 1)\left(C_{\varphi\ell}^{(1)ji} + C_{\varphi\ell}^{(3)ji}\right) + C_{\ell\ell}^{jijj}\right), \tag{32}$$

$$C_{VRR} = 2\left(2s_W^2 C_{\varphi e}^{ji} + C_{ee}^{jijj}\right), \tag{33}$$

$$C_{VLR} = -\frac{1}{2}C_{SRL} = 2s_W^2\left(C_{\varphi\ell}^{(1)ji} + C_{\varphi\ell}^{(3)ji}\right) + C_{\ell e}^{jijj}, \tag{34}$$

$$C_{VRL} = -\frac{1}{2}C_{SLR} = (2s_W^2 - 1)C_{\varphi e}^{ji} + C_{\ell e}^{jjji}, \tag{35}$$

$$C_{SLL} = C_{SRR} = C_{TL} = C_{TR} = 0, \tag{36}$$

$$C_{\gamma L} = \sqrt{2}C_\gamma^{ij\star}, \tag{37}$$

$$C_{\gamma R} = \sqrt{2}C_\gamma^{ji}, \tag{38}$$

where C_γ^{ji}, known as the photon dipole operator, is defined as

$$C_\gamma^{fi} \equiv \left(c_W C_{eB}^{fi} - s_W C_{eW}^{fi}\right) \tag{39}$$

and

$$\begin{aligned}X_\gamma = -\frac{16ev}{M}\text{Re}&\left[\left(2C_{VLL} + C_{VLR} - \frac{1}{2}C_{SLR}\right)C_{\gamma R}^\star \right. \\ & \left. + \left(2C_{VRR} + C_{VRL} - \frac{1}{2}C_{SRL}\right)C_{\gamma L}^\star\right] \\ & + \frac{64e^2v^2}{M^2}\left(\log\frac{M^2}{m^2} - \frac{11}{4}\right)(|C_{\gamma L}|^2 + |C_{\gamma R}|^2).\end{aligned} \tag{40}$$

D. Operators relevant for different LFV processes

In the model-independent approach of EFT, we either obtain the experimental constraints on the WCs or determine the nonzero value of those coefficients if there is an SM value-deviating signal. In order to do so, the renormalization group equations of the WCs of these relevant operators, represented as the combinations of anomalous-dimension (γ_{ij}) matrix of these dimension-six operators, need to be solved. These anomalous dimensions are defined as

$$\dot{C}_i \equiv 16\pi^2\mu\frac{dC_i}{d\mu} = \gamma_{ij}C_j. \tag{41}$$

Since flavor-changing effects are propagated through the Yukawa RGEs [119], we shall consider them in detail. There will be an additional 30 SMEFT operators, besides six primary operators, that contribute to LFVBD processes in different strengths. Therefore, it is useful to represent their contributions in a schematic form as

$$\begin{pmatrix} \dot{\boldsymbol{C}}_1 \\ \dot{\boldsymbol{C}}_2 \\ \dot{\boldsymbol{C}}_3 \\ \dot{\boldsymbol{C}}_4 \end{pmatrix}_Y \equiv 16\pi^2\mu\frac{d}{d\mu}\begin{pmatrix} \boldsymbol{C}_1 \\ \boldsymbol{C}_2 \\ \boldsymbol{C}_3 \\ \boldsymbol{C}_4 \end{pmatrix}_Y = \begin{pmatrix} \gamma_{11} & \gamma_{12} & 0 & 0 \\ \gamma_{21} & \gamma_{22} & \gamma_{23} & 0 \\ 0 & \gamma_{32} & \gamma_{33} & \gamma_{34} \\ 0 & 0 & \gamma_{43} & \gamma_{44} \end{pmatrix}_Y \begin{pmatrix} \boldsymbol{C}_1 \\ \boldsymbol{C}_2 \\ \boldsymbol{C}_3 \\ \boldsymbol{C}_4 \end{pmatrix}_Y, \tag{42}$$

with Y denoting the Yukawa RGEs and

$$(\boldsymbol{C}_1)_Y \equiv \left(C_{\ell q}^{(1)}, C_{\ell q}^{(3)}, C_{qe}, C_{\ell d}, C_{ed}, C_{\ell edq}\right)^T, \tag{43}$$

$$(\boldsymbol{C}_2)_Y \equiv \left(C_{\varphi q}^{(1)}, C_{\varphi q}^{(3)}, C_{\varphi\ell}^{(1)}, C_{\varphi\ell}^{(3)}, C_{\varphi d}, C_{\varphi e}, C_{\ell u}, C_{\ell e}, C_{eu}, C_{qq}^{(1)}, C_{qq}^{(3)}, C_{qd}^{(1)}, C_{qd}^{(8)}, C_{\ell equ}^{(1)}, C_{\ell equ}^{(3)}, C_{quqd}^{(1)}, C_{quqd}^{(8)}\right)^T, \tag{44}$$

$$(\boldsymbol{C}_3)_Y \equiv \left(C_{\varphi\Box}, C_{\varphi D}, C_{\varphi u}, C_{\varphi d}, C_{\varphi e}, C_{\varphi ud}, C_{ud}^{(1)}, C_{qu}^{(1)}, C_{qu}^{(8)}, C_{dd}, C_{\ell\ell}, C_{ee}\right)^T, \tag{45}$$

$$(\boldsymbol{C}_4)_Y \equiv (C_{uu})^T, \tag{46}$$

and $(\gamma_{ij})_Y$ represent the anomalous dimensions whose explicit forms, in terms of other WCs, are given in Ref. [120]. The form of the γ matrix in Eq. (42) tells us that RGEs of WCs of primary operators, mainly responsible for LFVBD and given by Eq. (43), depend on themselves and 17 other WCs listed in $\boldsymbol{C}_2$ [Eq. (44)]. These, in turn, depend on 12 other WCs besides themselves and similarly the single WC, C_{uu} in $\boldsymbol{C}_4$, completes the list of all WCs involved in LFVBD processes. These dependencies of WCs or operators are listed in $\boldsymbol{C}_2$, $\boldsymbol{C}_3$, and $\boldsymbol{C}_4$, respectively, and thus γ matrix elements bear nonzero contributions for all elements except γ_{13} and γ_{14}, as none of the operators listed in Eq. (43) depend on operators in Eq. (46). Table III represents the list of most relevant operators, or "primary operators," responsible for LFV processes under consideration in this analysis. In a similar fashion as described above, one can arrange and formulate the γ functions for all direct and induced operators for a particular LFV process.

IV. RESULTS AND DISCUSSION

We focus on probing new physics scenarios in a model-independent framework like SMEFT while primarily considering cLFV processes in B decays. Apart from the operators that directly affect the LFVBDs, we also consider a few relevant WCs associated with other LFV processes. We enumerate the operators associated with all the LFV processes considered in this analysis in Table III.

TABLE III. List of the dimension-six operators (invariant under the SM gauge group) that contribute to different LFV processes under consideration at the tree- or one-loop level.

Processes	Most relevant operators
$B \to K\ell_i\ell_j$	$\mathcal{O}_{\ell q}^{(1)}, \mathcal{O}_{\ell q}^{(3)}, \mathcal{O}_{qe}, \mathcal{O}_{\ell d}, \mathcal{O}_{ed}, \mathcal{O}_{\ell edq}$
$B \to K^*\ell_i\ell_j$	$\mathcal{O}_{\ell q}^{(1)}, \mathcal{O}_{\ell q}^{(3)}, \mathcal{O}_{qe}, \mathcal{O}_{\ell d}, \mathcal{O}_{ed}, \mathcal{O}_{\ell edq}$
$B_s \to \mu e$	$\mathcal{O}_{\ell q}^{(1)}, \mathcal{O}_{\ell q}^{(3)}, \mathcal{O}_{qe}, \mathcal{O}_{\ell d}, \mathcal{O}_{ed}, \mathcal{O}_{\ell edq}$
$\ell_i \to \ell_j\gamma$	$\mathcal{O}_{eB}, \mathcal{O}_{eW}$
$\ell_i \to \ell_j\ell_j\bar{\ell}_j$	$\mathcal{O}_{\varphi\ell}^{(1)}, \mathcal{O}_{\varphi\ell}^{(3)}, \mathcal{O}_{\varphi e}, \mathcal{O}_{\ell\ell}, \mathcal{O}_{\ell e}, \mathcal{O}_{ee}$
$\ell_i \to \ell_j\ell_k\bar{\ell}_k$	$\mathcal{O}_{\varphi\ell}^{(1)}, \mathcal{O}_{\varphi\ell}^{(3)}, \mathcal{O}_{\varphi e}, \mathcal{O}_{\ell\ell}, \mathcal{O}_{\ell e}, \mathcal{O}_{ee}$
$\mathrm{CR}(\mu \to e)$	$\mathcal{O}_{\varphi\ell}^{(1)}, \mathcal{O}_{\varphi\ell}^{(3)}, \mathcal{O}_{\varphi e}, \mathcal{O}_{eu}, \mathcal{O}_{\ell u}, \mathcal{O}_{\ell q}^{(1)}, \mathcal{O}_{\ell q}^{(3)}, \mathcal{O}_{qe}, \mathcal{O}_{\ell d}, \mathcal{O}_{ed}, \mathcal{O}_{\ell edq}, \mathcal{O}_{\ell equ}$
$Z \to \ell_i\ell_j$	$\mathcal{O}_{\varphi\ell}^{(1)}, \mathcal{O}_{\varphi\ell}^{(3)}, \mathcal{O}_{\varphi e}, \mathcal{O}_{eB}, \mathcal{O}_{eW}$
$\tau \to \mathcal{V}\ell$ $(\mathcal{V} = \rho, \phi)$	$\mathcal{O}_{\varphi\ell}^{(1)}, \mathcal{O}_{\varphi\ell}^{(3)}, \mathcal{O}_{\varphi e}, \mathcal{O}_{\ell u}, \mathcal{O}_{eu}, \mathcal{O}_{\ell equ}, \mathcal{O}_{eB}, \mathcal{O}_{eW}, \mathcal{O}_{\ell q}^{(1)}, \mathcal{O}_{\ell q}^{(3)}, \mathcal{O}_{qe}, \mathcal{O}_{\ell d}, \mathcal{O}_{ed}$
$\tau \to \mathcal{P}\ell$ $(\mathcal{P} = \pi^0, K^0)$	$\mathcal{O}_{\varphi\ell}^{(1)}, \mathcal{O}_{\varphi\ell}^{(3)}, \mathcal{O}_{\varphi e}, \mathcal{O}_{\ell u}, \mathcal{O}_{eu}, \mathcal{O}_{\ell equ}, \mathcal{O}_{eB}, \mathcal{O}_{eW}, \mathcal{O}_{\ell q}^{(1)}, \mathcal{O}_{\ell q}^{(3)}, \mathcal{O}_{qe}, \mathcal{O}_{\ell d}, \mathcal{O}_{ed}, \mathcal{O}_{\ell edq}$

As mentioned earlier, we compute the BRs of charged lepton flavor violating observables using the package FLAVIO [125]. The package WILSON [124] is used for the RGE running of the WCs. Remember that all the constraints used in this analysis (Table I) come from the upper limits of experimental data of the associated LFV processes rather than any explicit measurements having nonvanishing central values along with error estimates.

In the first part, we select the SMEFT WCs that are important for LFVBDs and probe the energy scale Λ from the experimental bounds of all the LFV processes. The associated WCs, considered one at a time at the scale Λ, are set to unity, whereas all the other WCs are set to zero at the same scale. Certainly, this involves (i) RGE running and the match and run procedure involving the SMEFT and the LEFT operators, as described earlier, and (ii) finding the low-energy observables for LFVBDs at the scale of m_b. The other LFV processes involve further smaller scales like m_τ or m_μ. We also remind ourselves that various WCs vanishing at the scale Λ may receive finite contributions at m_W due to RGE mixing. In this context, we will estimate the relative strengths of WCs in Table IV.

Going a step further, considering a fixed value of Λ, we will also consider several cases of two nonvanishing WCs and study the effects of the combined LFV constraints. We note that, while considering a given value of BR of a process, there may be three broad situations: (i) contributions from one of the WCs may be negligible, (ii) the same may be comparable to each other, and they add up constructively, and (iii) the same may interfere destructively. Plotted on a logarithmic scale, case (i) would result in contours almost parallel to one of the WC axes, case (ii) would produce round curves, whereas case (iii) would show up as cuspy regions. Clearly, in the last case, one

TABLE IV. Order of magnitude display of renormalization group evolved coupling strengths obtained at the energy scale $\mu = m_W$ for $\Lambda = 1$ TeV. The dark gray boxes with identical row and column indices refer to the WCs that are nonvanishing at the higher scale and prominent at m_W. Tiny coupling values below or equal to 10^{-14} appear in white boxes, whereas the values that are relatively prominent and above this limit are shown in light gray boxes.

WCs	$[C^{(1)}_{\ell q}]_{1223}$	$[C^{(3)}_{\ell q}]_{1223}$	$[C_{qe}]_{2312}$	$[C_{ed}]_{1223}$	$[C_{\ell d}]_{1223}$	$[C_{\ell edq}]_{1223}$	$[C^{(1)}_{\varphi\ell}]_{12}$	$[C^{(3)}_{\varphi\ell}]_{12}$	$[C_{\varphi e}]_{12}$
$[C^{(1)}_{\ell q}]_{1223}$	10^{-6}	10^{-8}	10^{-17}	10^{-24}	10^{-14}	10^{-16}	10^{-10}	10^{-11}	10^{-20}
$[C^{(3)}_{\ell q}]_{1223}$	10^{-8}	10^{-6}	10^{-19}	10^{-25}	10^{-16}	10^{-16}	10^{-12}	10^{-9}	10^{-23}
$[C_{qe}]_{2312}$	10^{-17}	10^{-18}	10^{-6}	10^{-14}	10^{-24}	10^{-18}	10^{-20}	10^{-22}	10^{-10}
$[C_{ed}]_{1223}$	10^{-23}	10^{-23}	10^{-13}	10^{-6}	10^{-17}	10^{-16}	10^{-27}	10^{-27}	10^{-17}
$[C_{\ell d}]_{1223}$	10^{-13}	10^{-15}	10^{-24}	10^{-17}	10^{-6}	10^{-14}	10^{-17}	10^{-19}	10^{-27}
$[C_{\ell edq}]_{1223}$	10^{-15}	10^{-14}	10^{-17}	10^{-15}	10^{-13}	10^{-6}	10^{-18}	10^{-18}	10^{-21}
$[C^{(1)}_{\varphi\ell}]_{12}$	10^{-9}	10^{-11}	10^{-20}	10^{-26}	10^{-16}	10^{-18}	10^{-6}	10^{-12}	10^{-17}
$[C^{(3)}_{\varphi\ell}]_{12}$	10^{-11}	10^{-9}	10^{-22}	10^{-27}	10^{-19}	10^{-18}	10^{-12}	10^{-6}	10^{-23}
$[C_{\varphi e}]_{12}$	10^{-19}	10^{-21}	10^{-9}	10^{-16}	10^{-26}	10^{-20}	10^{-17}	10^{-22}	10^{-6}
$[C_{\ell\ell}]_{1112}$	10^{-14}	10^{-15}	10^{-22}	10^{-30}	10^{-22}	10^{-21}	10^{-10}	10^{-9}	10^{-20}
$[C_{\ell e}]_{1112}$	10^{-20}	10^{-19}	10^{-15}	10^{-24}	10^{-27}	10^{-20}	10^{-20}	10^{-20}	10^{-10}
$[C_{\ell e}]_{1211}$	10^{-15}	10^{-14}	10^{-20}	10^{-27}	10^{-24}	10^{-21}	10^{-9}	10^{-12}	10^{-20}
$[C_{ee}]_{1112}$	10^{-22}	10^{-22}	10^{-14}	10^{-23}	10^{-30}	10^{-23}	10^{-20}	10^{-22}	10^{-9}
$[C_{eu}]_{1211}$	10^{-22}	10^{-22}	10^{-15}	10^{-24}	10^{-31}	10^{-24}	10^{-20}	10^{-22}	10^{-10}
$[C_{\ell u}]_{1211}$	10^{-15}	10^{-15}	10^{-22}	10^{-30}	10^{-24}	10^{-21}	10^{-10}	10^{-12}	10^{-20}
$[C^{(1)}_{\ell q}]_{1211}$	10^{-15}	10^{-15}	10^{-23}	10^{-30}	10^{-22}	10^{-21}	10^{-10}	10^{-11}	10^{-21}
$[C^{(3)}_{\ell q}]_{1211}$	10^{-14}	10^{-15}	10^{-23}	10^{-30}	10^{-22}	10^{-21}	10^{-13}	10^{-9}	10^{-23}
$[C_{qe}]_{1112}$	10^{-23}	10^{-23}	10^{-15}	10^{-22}	10^{-31}	10^{-24}	10^{-20}	10^{-21}	10^{-10}
$[C_{ed}]_{1211}$	10^{-23}	10^{-22}	10^{-15}	10^{-19}	10^{-29}	10^{-24}	10^{-20}	10^{-23}	10^{-10}
$[C_{\ell d}]_{1211}$	10^{-15}	10^{-15}	10^{-23}	10^{-29}	10^{-19}	10^{-21}	10^{-10}	10^{-12}	10^{-20}
$[C_{\ell edq}]_{1211}$	10^{-19}	10^{-18}	10^{-21}	10^{-25}	10^{-23}	10^{-16}	10^{-19}	10^{-18}	10^{-22}
$[C_{\ell edq}]_{1222}$	10^{-19}	10^{-17}	10^{-23}	10^{-19}	10^{-16}	10^{-9}	10^{-17}	10^{-17}	10^{-21}
$[C^{(1)}_{\ell equ}]_{1211}$	10^{-19}	10^{-19}	10^{-21}	10^{-28}	10^{-26}	10^{-19}	10^{-19}	10^{-19}	10^{-22}
$[C_{eB}]_{12}$	10^{-15}	10^{-14}	10^{-17}	10^{-25}	10^{-23}	10^{-17}	10^{-16}	10^{-15}	10^{-18}
$[C_{eB}]_{21}$	10^{-17}	10^{-17}	10^{-15}	10^{-23}	10^{-25}	10^{-26}	10^{-18}	10^{-18}	10^{-16}
$[C_{eW}]_{12}$	10^{-15}	10^{-14}	10^{-17}	10^{-25}	10^{-22}	10^{-17}	10^{-16}	10^{-15}	10^{-18}
$[C_{eW}]_{21}$	10^{-17}	10^{-17}	10^{-15}	10^{-22}	10^{-25}	10^{-26}	10^{-18}	10^{-18}	10^{-16}

requires larger absolute values of both the WCs and the associated regions correspond to the so-called "flat directions."

A. Single operator analysis

As mentioned earlier, in this part we choose a single WC initialized to unity at the SMEFT scale of $\mu = \Lambda$ and evolve it toward a low-scale m_W via appropriate RGEs. We will set all other WCs to zero at Λ. Based on our earlier discussion on LFVBDs, we have the following single operator scenarios where WCs of primary importance are $[C_{\ell q}^{(1,3)}]_{\ell\ell'23}$, $[C_{qe}]_{\ell\ell'23}$, $[C_{ed}]_{\ell\ell'23}$, $[C_{\ell d}]_{\ell\ell'23}$, and $[C_{\ell edq}]_{\ell\ell'23}$. Here, $\ell\ell' \in (12, 13, 23)$ represents the combinations $e-\mu$, $e-\tau$ and $\mu-\tau$, respectively. At the low-energy scale, the first three WCs, namely, $[C_{\ell q}^{(1)}]_{\ell\ell'23}$, $[C_{\ell q}^{(3)}]_{\ell\ell'23}$, and $[C_{qe}]_{\ell\ell'23}$, contribute to left-handed $C_{9,10}$, the next two contribute to right-handed $C'_{9,10}$, and the last one and its chiral counterpart relate to $C_{S,P}$ and $C'_{S,P}$ of LFVBDs, respectively [Eqs. (13)–(18)].

As indicated by the RGEs [Eqs. (41)–(46)], WCs of different operators mix among themselves, and a given vanishing WC at a high-energy scale may accumulate a nonzero value at a low-energy scale like m_W. Furthermore, it is necessary to explore the mutual dependence of the primarily important WCs associated with the LFVBDs and a few of the WCs important for the other LFV processes due to RGE effects. Thus, we choose to study the above effects of all the WCs grouped under $\boldsymbol{C_{1Y}}$ [Eq. (43)] and $C_{\varphi\ell}^{(1)}$, $C_{\varphi\ell}^{(3)}$, and $C_{\varphi e}$ of $\boldsymbol{C_{2Y}}$ [Eq. (44)] that are relevant from Table III. This leads to Table IV where we show the depiction of order of magnitudes of the said WCs due to RGE effects, while ignoring signs. We use $\Lambda = 1$ TeV and set the desired nonvanishing WC to unity at the same scale, indicating a coupling (C/Λ^2) value of 10^{-6} GeV^{-2}, where C refers to a given WC. The first nine rows and nine columns of Table IV show the interdependence of the said WCs. Additionally, from the tenth row onward, we explore the effects on a few more WCs that are relevant in the context of the other LFV processes (Table III). All coupling entries in the table are obtained at the energy scale $\mu = m_W$. The dark gray boxes with identical row and column indices refer to the WCs that are nonvanishing at the higher scale and prominent at m_W. Tiny coupling values below or equal to 10^{-14} appear in white boxes, whereas the values that are relatively prominent and above this limit are shown in light gray boxes. For example, focusing on the $C_{\ell q}^{(1)}$ column, the RGE effects have significant impacts on $C_{\ell q}^{(3)}$, $C_{\varphi\ell}^{(1)}$, and $C_{\varphi\ell}^{(3)}$. However, the same on the rest of the WCs is hardly significant. A similar behavior holds true for $C_{\ell q}^{(3)}$ as well. Moreover, both $C_{\ell q}^{(1)}$ and $C_{\ell q}^{(3)}$ can also affect the dipole operators C_{eW} and C_{eB}, which are quite important in the context of the stringent limit from $\mu \to e\gamma$. Considering C_{qe}, we find that it has a relatively prominent RGE impact on $C_{\varphi e}$, whereas for C_{ledq} the scenario is little different. In this case, the relevant WC (with specific quark indices) is $[C_{ledq}]_{1223}$, which has significant impact only on $[C_{ledq}]_{1222}$ (i.e., with different quark indices).

In Figs. 2 and 3, we probe the maximum attainable energy scales denoted as Λ by considering the sensitivities of operators relevant to LFV processes (Table I). We consider the current experimental limits to probe Λ and see any prospective change in conclusion by using possible future bounds of the same processes. We choose the operators that directly affect the LFVBD processes and constrain Λ by those, as well as via other LFV limits. We vary a coupling by changing the scale Λ while fixing the associated WC to unity at that scale. The x axes in these bar diagrams display the BRs associated with different LFV processes, while the y axes represent the requisite energy scale Λ maximally consistent with the BRs from the table. For a given operator, each LFV process may, at most, be shown via a bar with two distinct colors: blue color within the bar indicating the current experimental bound on the BRs, and the green color representing the anticipated future constraint on the same as mentioned in the table. Among the LFVBDs, the processes that have definite future sensitivity predictions for BRs like $B_s \to \mu^+ e^-$, the color codes continue to remain the same. Additionally, we extend our studies to probe how robust would be our conclusions in the presence of a higher degree of sensitivities for some of the LFVBDs, like $B^+ \to K^+\mu^+e^-$ or $B^0 \to K^{*0}\mu^+e^-$. Accordingly, we use darker and lighter shadings of red to correspond to sensitivity enhancement by 2 and 4 orders of magnitude, respectively. This extended analysis is indeed performed in the same spirit of the recent work of Ref. [117]. The above levels of sensitivity of the mentioned LFVBDs place the latter on the same footing as with the predicted improvements of BRs of the other LFV processes.

In the top row of Fig. 2, we choose three WCs, namely, $C_{\ell q}^{(1)}$, $C_{\ell q}^{(3)}$, and C_{qe} that are most relevant for LFVBDs, as well as those that can influence other LFV processes significantly, although indirectly. On the other hand, C_{ed} and $C_{\ell d}$ do not have enough RGE running effects to have influence on the other LFV processes, hence these are omitted in this study. As shown in Fig. 2, the LFVBDs like $\mathcal{B}(B^+ \to K^+\mu e)$, followed by $\mathcal{B}(B^0 \to K^{*0}\mu e)$ and $\mathcal{B}(B_s \to \phi\mu e)$, have similar values of Λ, thus they are quite equally constraining. On the other hand, the effect from $\mathcal{B}(B_s \to \mu e)$ is quite less significant. Among other LFV decays, $\mathrm{CR}(\mu \to e)$, followed by $\mu \to eee$ provide the most significant constraints to these WCs. Additionally, the ability of $Z \to \mu e$ to constrain these sets of WCs is hardly of any significance. Similarly, in the bottom panel of Fig. 2, for $C_{\ell edq}$ (considering both flavor indices 1223 and 2132), we observe that the current constraints predominantly originate from LFVBDs, particularly from processes such

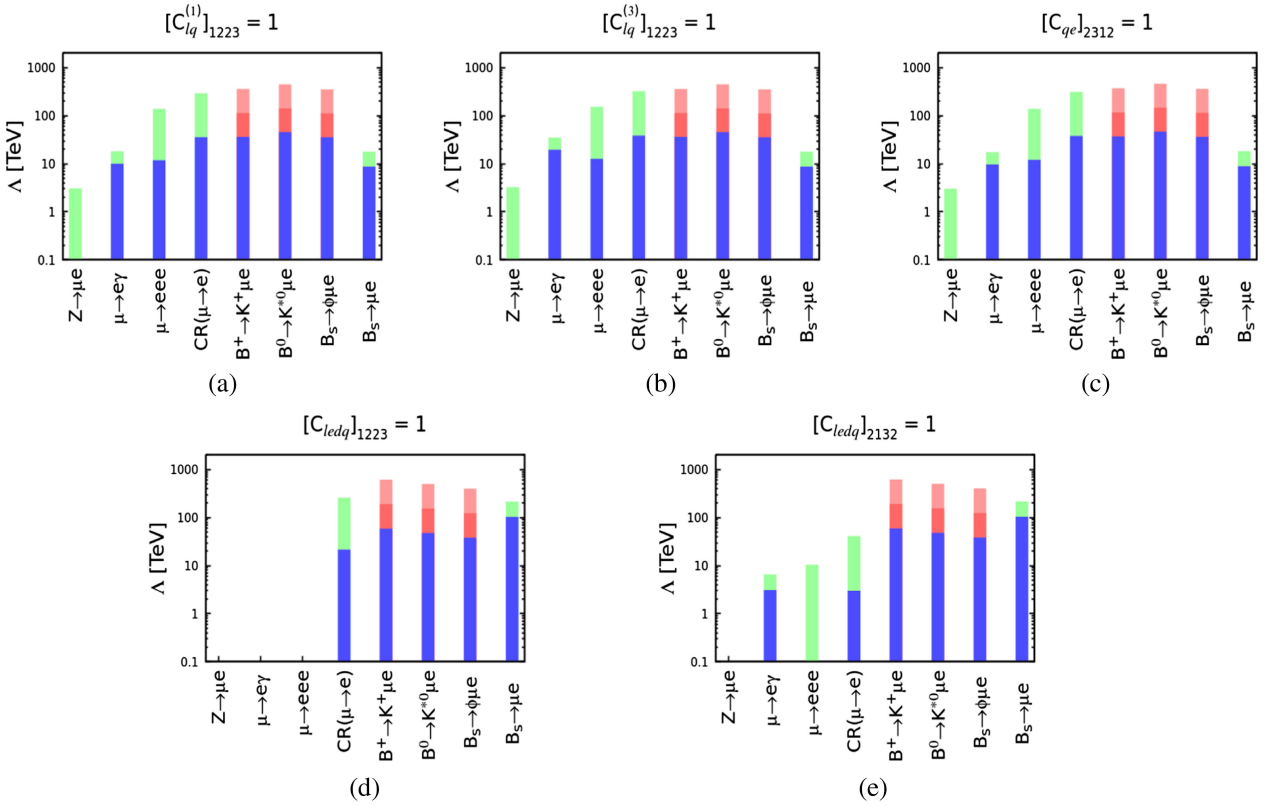

FIG. 2. Display of values of Λ for (a) $C_{\ell q}^{(1)}$, (b) $C_{\ell q}^{(3)}$, (c) C_{qe} (in the top row) and (d) and (e) $C_{\ell edq}$ (in the bottom row), for $\mu - e$, that are consistent with the present and future experimental bounds of various LFV decays when only one single (perturbative) WC is fixed at unity. Blue and green bars refer to current and possible future bounds of LFV processes, respectively, as described in Table I. Darker and lighter red shades, starting above the blue shades, represent the assumed enhancement of the BR sensitivity by 2 and 4 orders of magnitude, respectively.

as $\mathcal{B}(B_s \to \mu e)$, rather than from $\mathcal{B}(B \to K^{(*)}\mu e)$. This distinction arises due to the varying combinations of prefactors associated with $C_{\ell edq}$, a fact that can be verified by referring to Eqs. (47) and (48). In regard to the same process, looking at the numerical values of the bar diagrams of Fig. 2, we find that the orders of magnitude of the BRs for LFVBDs in scenarios involving $C_{\ell q}^{(1)}$, $C_{\ell q}^{(3)}$, and C_{qe} are quite similar and challenging to distinguish, however, $C_{\ell edq}$ probes a higher energy scale.

When turning our attention to the anticipated future constraints referred to in Table I (green shades in bar diagrams), we find that $\mathrm{CR}(\mu \to e)$, followed by $\mu \to eee$ to provide significant bounds on the above sets of WCs. Although there is no direct correlation between $C_{\ell q}^{(1)}$, $C_{\ell q}^{(3)}$, C_{qe}, and these LFV processes, the RGE running effects play crucial roles in enhancing the effect of the constraints imposed by $\mathrm{CR}(\mu \to e)$ and $\mu \to eee$. This happens due to the influence of Higgs-lepton WCs. Consequently, the future bound for $\mu \to eee$ sets a cutoff on the energy scale Λ at ∼138 TeV (as obtained from our numerical analysis) for $C_{\ell q}^{(1)}$ and $C_{\ell q}^{(3)}$, while $\mathrm{CR}(\mu \to e)$ (phase II) establishes a cutoff ∼291 TeV. On the other hand, if we consider the assumed future sensitivities of BRs for some of the LFVBDs (lighter and darker red shades), we find that the dominant constraints come from LFVBDs. Similarly for C_{qe}, one has $\Lambda \simeq 313$ TeV from $\mathrm{CR}(\mu \to e)$ (phase II), whereas it coincides with the scales associated with $C_{\ell q}^{(1)}$ and $C_{\ell q}^{(3)}$ when derived from $\mu \to eee$.

Furthermore, investigating the expected future bounds on $C_{\ell edq}$ as depicted in the bottom row of Fig. 2, we observe that the most stringent constraint emanates from $\mathcal{B}(B_s \to \mu e)$, effectively placing a cutoff on the energy scale Λ at around 330 TeV. For other LFV decays, the future bound of $\mathrm{CR}(\mu \to e)$ closely aligns with the prospective bound of $\mathcal{B}(B_s \to \mu e)$, specifically for $[C_{\ell edq}]_{1223}$. This correlation arises due to the RGE effects that significantly contribute to $[C_{\ell edq}]_{1222}$, thereby directly bolstering the constraints imposed by $\mathrm{CR}(\mu \to e)$. However, the situation differs when considering $[C_{\ell edq}]_{2132}$, where there exist only some mild RGE effects. A distinction between $[C_{\ell edq}]_{1223}$ and $[C_{\ell edq}]_{2132}$ emerges in that the latter contributes additionally to $\mu \to e\gamma$ and $\mu \to eee$. The associated RGEs of the WCs when examined reveal that the latter contribute to the dipole operators, specifically $\mathcal{O}_{eB}$ and $\mathcal{O}_{eW}$, which in turn make substantial contributions to these LFV processes. It is important to note that, while the current constraints from the processes such as

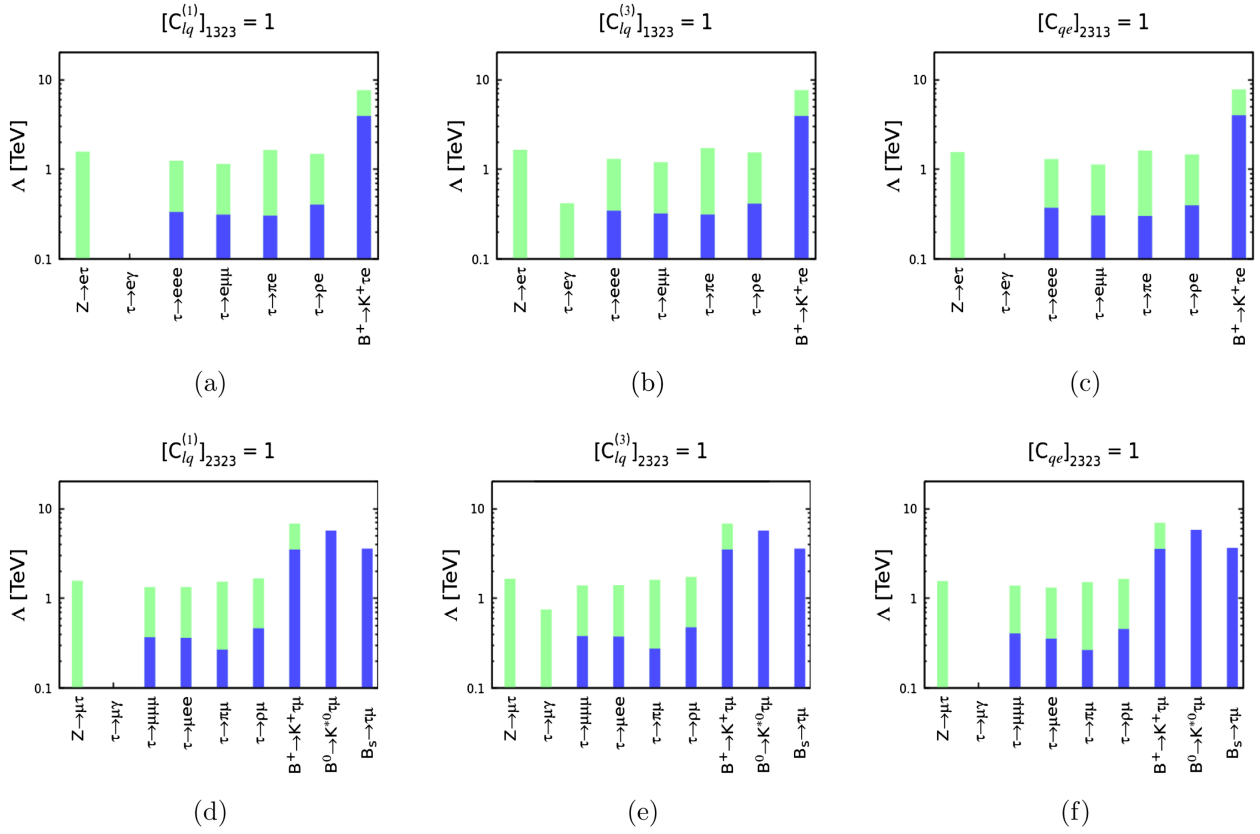

FIG. 3. Similar as Fig. 2 for $e-\tau$ (in the top row) and $\mu-\tau$ (in the bottom row).

$\mathrm{CR}(\mu \to e)$, $\mu \to eee$, and $\mu \to e\gamma$ are significant, the corresponding energy scales remain below the ones established by LFVBDs. Nevertheless, if the sensitivities of the LFVBDs other than $\mathcal{B}(B_s \to \mu e)$ can be enhanced by 2–4 orders of magnitude (shown in red shades), one can probe the new physics energy scale ∼100 TeV, which is higher than the same probed by $\mathrm{CR}(\mu \to e)$ for both $[C_{\ell edq}]_{1223}$ and $[C_{\ell edq}]_{2132}$. Therefore, if new physics primarily generates the LFVBD operators above 100 TeV, we expect that $B^0 \to K^{*0}\mu^+e^-, B^+ \to K^+\mu^+e^-$, $B_s \to \phi\mu^-e^+, B_s \to \mu^+e^-$, and $\mathrm{CR}(\mu \to e)$ to be quite promising in regard to future experiments.

We now like to enumerate the relative importance of the LFV constraints within the $\mu-\tau$ and $e-\tau$ sectors. While examining the current constraints within the said sectors (with flavor indices 2323 and 1323) as obtained in Fig. 3, we find that the most stringent limitations on the WCs $C_{\ell q}^{(1)}$, $C_{\ell q}^{(3)}$, and C_{qe} primarily arise from LFVBDs. There is hardly any necessity to perform an extended sensitivity analysis for the τ sector. The reason being, in the $\mu-\tau$ and $e-\tau$ sectors, even the most optimistic future sensitivities of BRs for all the other LFVs lie below the present limits of any of the LFVBDs. Additionally, the average reach of the excluded energy scales for these operators is much smaller compared to the same for the $e-\mu$ sector. However, if $2q2\ell$ operators serve as the primary source of lepton flavor violation at the NP scale, we can constrain the other LFV processes using results of this sector of LFVBDs. In this context, as displayed in Table IV, we remind the reader that the WCs $C_{\ell q}^{(1)}$, $C_{\ell q}^{(3)}$, and C_{qe} responsible for LFVBDs contribute significantly to the Higgs-lepton WCs $(C_{\varphi\ell}^{(1)}, C_{\varphi\ell}^{(3)}, C_{\varphi e})$ through the RGE running. We refer to Table V for the bounds on the BRs of other LFV processes from the strongest bound available from the future limit of $\mathcal{B}(B^+ \to K^+\mu\tau)$ corresponding to the three WCs $C_{\ell q}^{(1)}$, $C_{\ell q}^{(3)}$, and C_{qe}. We find that the order of magnitude of BRs in all the processes is nearly $(\sim 10^{-12})$, which is almost 3–4 orders below the expected bounds reported by the respective experiments. In regard to $\tau \to \mu\gamma$ and $\tau \to e\gamma$, there are hardly any contributions from $C_{\ell q}^{(1)}$ and C_{qe} compared to $C_{\ell q}^{(3)}$, a fact that can be attributed to the RGEs of these WCs.

Coming back to the $e-\mu$ sector, we now like to explore the prospect of constraining LFVBDs via the relevant WCs $C_{\ell q}^{(1)}$, $C_{\ell q}^{(3)}$, C_{qe}, and $C_{\ell edq}$ while considering the future limits of $\mu \to eee$, and $\mathrm{CR}(\mu \to e)$ (phases I and II). The requirement for finding these numbers in Table VI is that the BRs of these processes, which are also induced by the WCs listed in column 2 of the same table, should lie below their future limits. Therefore, focusing on these

TABLE V. Indirect upper limits on the BRs of the other LFV processes in the $\mu - \tau$ sector, obtained from the future limit of $\mathcal{B}(B^+ \to K^+\mu\tau)$ (strongest constraint) in the 1D scenario.

Operator	$\mathrm{BR}(Z \to \mu\tau)$	$\mathrm{BR}(\tau \to \mu\gamma)$	$\mathrm{BR}(\tau \to \mu\mu\mu)$	$\mathrm{BR}(\tau \to \mu ee)$	$\mathrm{BR}(\tau \to \pi\mu)$	$\mathrm{BR}(\tau \to \rho\mu)$
$[C_{\ell q}^{(1)}]_{2323}$	5.7×10^{-12}	2.5×10^{-13}	1.3×10^{-12}	9.7×10^{-13}	2.6×10^{-12}	1.4×10^{-12}
$[C_{\ell q}^{(3)}]_{2323}$	7.2×10^{-12}	2.2×10^{-12}	1.7×10^{-12}	1.2×10^{-12}	3.2×10^{-12}	1.7×10^{-12}
$[C_{qe}]_{2323}$	5.0×10^{-12}	2.1×10^{-13}	1.3×10^{-12}	8.5×10^{-13}	2.3×10^{-12}	1.3×10^{-12}

TABLE VI. Indirect upper limits from $\mu \to eee$, $\mathrm{CR}(\mu \to e, \mathrm{Al})$ phases I and II on different LFVBD processes considering a single operator responsible for such processes, at the scale $\mu = \Lambda$. See text for the absence of data for $C_{\ell edq}$.

Observable	WC	UL from $\mathrm{BR}(\mu \to eee)$	UL from $\mathrm{CR}(\mu \to e, \mathrm{Al})$, phase I	UL from $\mathrm{CR}(\mu \to e, \mathrm{Al})$, phase II
$\mathrm{BR}(B^+ \to K^+\mu^-e^+)$	$[C_{\ell q}^{(1)}]_{1223}$	2.9×10^{-11}	2.2×10^{-10}	1.5×10^{-12}
	$[C_{\ell q}^{(3)}]_{1223}$	1.9×10^{-11}	1.5×10^{-10}	9.8×10^{-13}
	$[C_{qe}]_{2312}$	3.2×10^{-11}	1.8×10^{-10}	1.2×10^{-12}
	$[C_{ledq}]_{1223}$	⋯	⋯	1.9×10^{-11}
$\mathrm{BR}(B^0 \to K^{*0}\mu^-e^+)$	$[C_{\ell q}^{(1)}]_{1223}$	6.3×10^{-11}	4.7×10^{-10}	3.4×10^{-12}
	$[C_{\ell q}^{(3)}]_{1223}$	4.2×10^{-11}	3.3×10^{-10}	2.3×10^{-12}
	$[C_{qe}]_{2312}$	6.9×10^{-11}	3.8×10^{-10}	2.9×10^{-12}
	$[C_{ledq}]_{1223}$	⋯	⋯	7.9×10^{-12}
$\mathrm{BR}(B_s \to \phi\mu^-e^+)$	$[C_{\ell q}^{(1)}]_{1223}$	6.7×10^{-11}	4.9×10^{-10}	3.4×10^{-12}
	$[C_{\ell q}^{(3)}]_{1223}$	4.5×10^{-11}	3.5×10^{-10}	2.3×10^{-12}
	$[C_{qe}]_{2312}$	7.5×10^{-11}	4.1×10^{-10}	2.8×10^{-12}
	$[C_{ledq}]_{1223}$	⋯	⋯	8.6×10^{-12}
$\mathrm{BR}(B_s \to \mu^-e^+)$	$[C_{\ell q}^{(1)}]_{1223}$	8.0×10^{-14}	5.9×10^{-13}	4.0×10^{-15}
	$[C_{\ell q}^{(3)}]_{1223}$	5.3×10^{-14}	4.2×10^{-13}	2.7×10^{-15}
	$[C_{qe}]_{2312}$	8.9×10^{-14}	4.9×10^{-13}	3.4×10^{-15}
	$[C_{ledq}]_{1223}$	⋯	⋯	1.4×10^{-10}

numbers we observe that, from the future bounds of $\mathrm{CR}(\mu \to e)$ (phase I), in scenarios like $C_{\ell q}^{(1)}$, $C_{\ell q}^{(3)}$, and C_{qe}, the upper limits of $\mathcal{B}(B \to K^{(*)}\mu e)$ and $\mathcal{B}(B_s \to \phi\mu e)$ ($\sim 10^{-10}$) are smaller by 1 order of magnitude compared to the current experimental bounds. It is interesting to note that these numbers fall within the scope of the future bounds that are expected to be obtained through upgrades at LHCb and Belle II as discussed in Sec. I. This also falls within a two-order smaller LFVBDs zone as explored in this work. However, the situation is notably different for $\mathcal{B}(B_s \to \mu e)$, since the above-mentioned WCs predict too low BRs that are way beyond the reach of B factories. This is in contrast to the case of $C_{\ell edq}$ scenarios. Here, considering limits as obtained from $\mathrm{CR}(\mu \to e)$ (phase I), the BR bounds LFVBDs are significantly higher than the current limits, and no data are shown in this regard. For the process $\mu \to eee$ in regard to $C_{\ell q}^{(1)}$, $C_{\ell q}^{(3)}$, and C_{qe} we also observe a similar pattern of a lowered BR. The bounds obtained from $\mu \to eee$ are about 1 order of magnitude stronger than those from $\mathrm{CR}(\mu \to e)$ (phase I), allowing for even tighter constraints on the BRs of LFVBDs. We point out that the $C_{\ell edq}$ scenarios do not affect $\mu \to eee$ through RGEs, thus there are no data corresponding to its entries in the $\mu \to eee$ column of Table VI.

Moving forward, the predicted future bound of $\mathrm{CR}(\mu \to e)$ (phase II) provides the most stringent constraints on these WCs compared to the other two scenarios. Consequently, for $C_{\ell q}^{(1)}$, $C_{\ell q}^{(3)}$, and C_{qe}, the indirect upper limit (UL) on the BRs of LFVBDs is further reduced by several orders of magnitude for $\mathcal{B}(B \to K^{(*)}\mu e)$, $\mathcal{B}(B_s \to \phi\mu e)$, and $\mathcal{B}(B_s \to \mu e)$ compared to the current limits. However, in the case of $C_{\ell edq}$, a slightly different

pattern emerges. The indirect ULs obtained in this scenario for $\mathcal{B}(B \to K^{(*)}\mu e)$ and $\mathcal{B}(B_s \to \phi\mu e)$ decays are $\sim 10^{-12}$, while for $\mathcal{B}(B_s \to \mu e)$ the UL is $\sim 10^{-10}$. The later UL aligns with the anticipated future limit proposed by LHCb-II (Table I).

B. Two operator interference

In this section, we discuss the effects when two operators are turned on at the high-energy scale Λ, particularly in relation to how their mutual interference can affect the different LFV observables including LFVBDs. Prime motivations for such analysis are twofold. First, we can analyze the operator mixing and interplay of RGE flows among the operators that are responsible exclusively for LFVBDs. Second, we can estimate the effects of the nontrivial cancellations due to appropriately chosen different pairs of WCs that appear in the BR formulas of LFV processes of interest. Since WCs are related to each other via RGEs, they can combine in different strengths to suppress or enhance concerned LFV processes.

In the plane of a pair of WCs, the so-called flat directions are defined as the portions of the contour where there is a cancellation from the contributing terms within the BR arising from these WCs [115]. In such scenarios, it is also possible to tune the parameters to enhance the relative strengths of LFV processes. Such relations can easily be found from the BR formula of the corresponding LFV process and they would appear as cuspy regions in the two-dimensional plots in this analysis. For our purpose, from Eqs. (11) and (12), corresponding forms of WCs given in Eqs. (13)–(17) and considering only the relevant operators that contribute to LFVBDs, we find that

$$\begin{aligned}&\mathrm{Br}\left[B_s \to \ell_i^+ \ell_j^-\right] \\ &\sim k_1\left\{k_2\left(C^{(1)}_{\ell q} + C^{(3)}_{\ell q} + C_{qe}\right) + k_3\left(C_{\ell edq} - C'_{\ell edq}\right)\right\}^2 \\ &\quad + k_4\left\{k_5\left(C^{(1)}_{\ell q} + C^{(3)}_{\ell q} - C_{qe}\right) + k_6\left(C_{\ell edq} + C'_{\ell edq}\right)\right\}^2, \end{aligned} \tag{47}$$

$$\begin{aligned}\mathrm{Br}\left[B^0 \to K^{(*)}\ell_i^+ \ell_j^-\right] \sim\ & k_7\left\{\left(C^{(1)}_{\ell q} + C^{(3)}_{\ell q}\right)^2 + \left(-C_{qe}\right)^2\right\} \\ & + k_8\left\{\left(C^{(1)}_{\ell q} + C^{(3)}_{\ell q}\right)^2 + \left(C_{qe}\right)^2\right\} \\ & + k_9\left(C_{\ell edq} - C'_{\ell edq}\right)^2, \end{aligned} \tag{48}$$

where k_i's refer to appropriate products from Eq. (11). Considering 2D cases, the above equations show that, for both types of LFVBD processes, one may have interfering terms containing a pair of WCs.

In the following discussion, depending on the possibility of having flat directions in the BRs, we analyze below five different 2D scenarios. Among them, we study the cancellation within the pair of WCs responsible for LFVBDs in the first three scenarios. For this, we simultaneously consider the presence of two nonzero coefficients of $2q2\ell$ operators relevant for LFVBDs at the scale Λ. Considering the operators with significant effects to LFVBDs and using Eq. (47) and (48) as our guiding principle, we choose the scenarios with ($[C^{(1)}_{\ell q}]_{1223}$, $[C^{(3)}_{\ell q}]_{1223}$), ($[C_{\ell edq}]_{2132}$, $[C^{(1)}_{\ell q}]_{1223}$), and ($[C_{\ell edq}]_{1223}$, $[C_{qe}]_{2312}$). Similarly, to study the possibility of nontrivial cancellations, we simultaneously consider (i) the presence of a nonzero coefficient of $2q2\ell$ operators relevant for LFVBDs (either one from $[C^{(1,3)}_{\ell q}]_{1223}$, $[C_{qe}]_{2312}$, $[C_{\ell edq}]_{1223}$) and (ii) nonvanishing Higgs-lepton operators that are relevant for $\mu \to eee$, $\mathrm{CR}(\mu \to e, \mathrm{Al})$.

Figure 4 illustrates the contours of $\mathcal{B}(B^0 \to K^{*0}\mu e)$, $\mu \to eee$, and $\mathrm{CR}(\mu \to e)$ in the plane of WCs $[C^{(1)}_{\ell q}]_{1223}$ and $[C^{(3)}_{\ell q}]_{1223}$, both referring to the energy scale $\Lambda = 1$ TeV. It is observed that similar results hold true also for higher values of Λ, with only minor logarithmic modifications due to RGEs. Lighter colors show the currently allowed regions for $\mu \to eee$ (brown) and $\mathrm{CR}(\mu \to e)$ (blue) experiments, whereas darker shades of the same colors represent futuristic experimental limits tabulated in Table I. For $\mathrm{CR}(\mu \to e)$, we differentiate between two future expectations: the slightly lighter blue shade corresponds to phase I ($\mathrm{BR} \sim 10^{-15}$) as proposed by J-PARK and Fermilab [130] and the darker blue shade corresponds to phase II ($\mathrm{BR} \sim 10^{-17}$ [130]). The contours for $B^0 \to K^{*0}\mu e$ are shown in black, with the solid line indicating the current limit ($\mathrm{BR} \sim 10^{-9}$), which is also the most stringent limit among these three processes for this set of WCs. However, the future predictions for $\mu \to eee$ and $\mathrm{CR}(\mu \to e)$ (phase I) impose stronger constraints on both $[C^{(1)}_{\ell q}]_{1223}$ and $[C^{(3)}_{\ell q}]_{1223}$. Notably, $\mu \to eee$ surpasses phase I of $\mathrm{CR}(\mu \to e)$ in terms of constraining these WCs. The new parameter space constrained by $\mu \to eee$ for this set of WCs reduces $\mathcal{B}(B^0 \to K^{*0}\mu e)$ by 1 order of magnitude from the existing bound. Belle II and LHCb experiments can potentially probe this limit. Moreover, $\mathrm{CR}(\mu \to e)$ (phase II) impose the strongest constraints on the parameter space of $[C^{(1)}_{\ell q}]_{1223}$ and $[C^{(3)}_{\ell q}]_{1223}$, causing $\mathcal{B}(B^0 \to K^{*0}\mu e)$ to shrink 2–3 orders of magnitude from the existing bound. However, achieving this level of BR is very challenging given the current and the upcoming scopes of B factories in the near future. The plot in the $[C^{(1)}_{\ell q}]_{1223}$ and $[C^{(3)}_{\ell q}]_{1223}$ plane also provides insights into the flat directions among all three LFV processes. The flat direction for $B^0 \to K^{0*}\mu e$ falls in the second quadrant and the associated cancellation

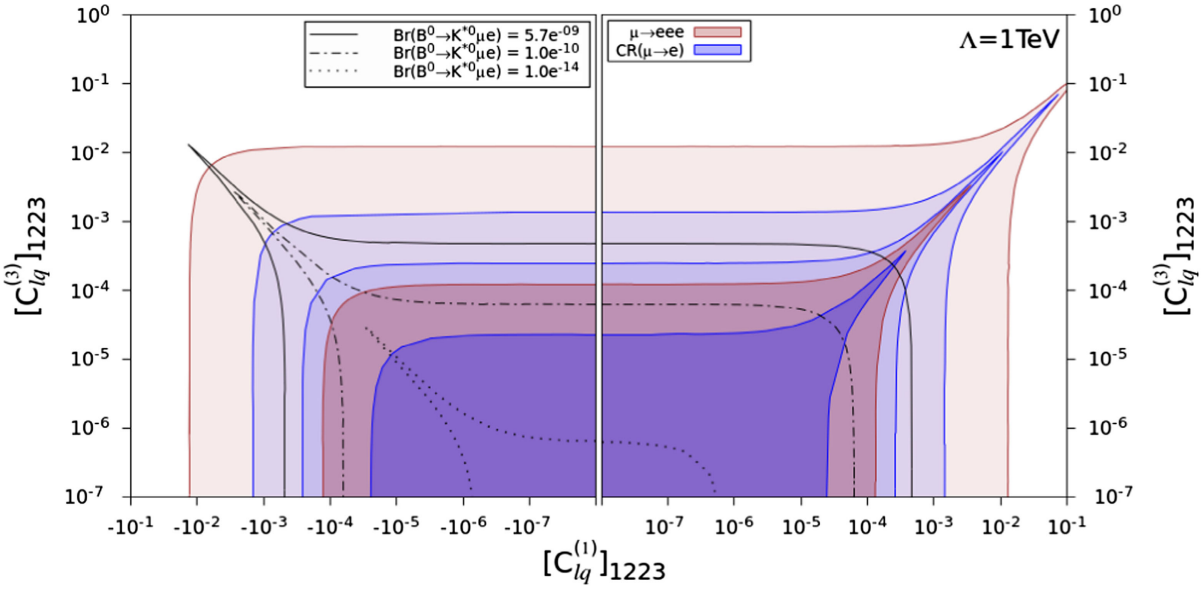

FIG. 4. With $\Lambda = 1$ TeV, contours for $B^0 \to K^{*0}\mu e$ as a function of $[C^{(1)}_{\ell q}]_{1223}$ and $[C^{(3)}_{\ell q}]_{1223}$. Lighter colors show the currently allowed regions for $\mu \to eee$ (brown) and $\mathrm{CR}(\mu \to e)$ (blue) bounds, whereas darker shades represent futuristic limits. For $\mathrm{CR}(\mu \to e)$, the lighter and darker blue shades correspond to phase I ($\mathrm{BR} \sim 10^{-15}$) and phase II ($\mathrm{BR} \sim 10^{-17}$), respectively.

is consistent with Eq. (48). In contrast, for the other LFV processes, namely, $\mu \to eee$ and $\mathrm{CR}(\mu \to e)$, cancellations occur on the opposite side. We note that the processes like $\mu \to eee$ and $\mathrm{CR}(\mu \to e)$ exhibit flat directions resulting from cancellations between $[C^{(1)}_{\phi\ell}]_{12}$ and $[C^{(3)}_{\phi\ell}]_{12}$ and this is induced by the RGE flows. The latter can be understood by analyzing the running and matching of SMEFT and LEFT operators. Using appropriate results from Sec. III, we find

$$\left[C^{(1)}_{\phi\ell}(\mu) + C^{(3)}_{\phi\ell}(\mu)\right]_{12} \approx \frac{3Y_c Y_t}{8\pi^2}\log\left(\frac{\mu}{\Lambda}\right) \times \left[C^{(1)}_{\ell q}(\Lambda) - C^{(3)}_{\ell q}(\Lambda)\right]_{1223}. \quad (49)$$

The presence of heavy Yukawa terms with top quark in Eq. (49) represents the fact that large Higgs-lepton operators can be induced by the $2q2\ell$ operators, even though they were absent at the starting scale Λ. Additionally, in regard to the contours corresponding to $\mu \to eee$ and $\mathrm{CR}(\mu \to e)$, cuspy regions arise in the first quadrant of the figure drawn in the $C^{(1)}_{\ell q} - C^{(3)}_{\ell q}$ plane. Thus, a small value of the right hand side of Eq. (49) for the said region corresponds to a small value for the sum $C^{(1)}_{\phi\ell}(\mu) + C^{(3)}_{\phi\ell}(\mu)$. It may easily be seen that the same would appear in the BR formulas of $\mu \to eee$ and $\mathrm{CR}(\mu \to e)$, which, in turn, means a flat direction or cancellation of appropriate terms induced by RGE effects. A close examination of the plot also reveals that the cuspy region resulting from the current limit of $B^0 \to K^{*0}\mu e$ mildly constrains the parameter space allowed by future bounds of $\mu \to eee$ and $\mathrm{CR}(\mu \to e)$ (phase I). Similarly, the cuspy region stemming from the current bound of $\mathrm{CR}(\mu \to e)$ limits some of the regions allowed by the $B \to K^{*0}\mu e$ contour. Likewise, the converse is true in the left quadrant.

Figure 5 represents the contours of $\mathcal{B}(B_s \to \mu e), \mu \to eee$ and $\mathrm{CR}(\mu \to e)$, in the plane of WCs $[C'_{\ell edq}]_{1223}$ vs $[C^{(1)}_{\ell q}]_{1223}$ (top) and $[C_{\ell edq}]_{2132}$ vs $[C_{qe}]_{2312}$ (bottom), both corresponding to the energy scale $\Lambda = 1$ TeV. All the colored contours have similar classifications as described in the above paragraph. One noteworthy aspect of these WCs is that, at the low-energy limit m_b, they simultaneously influence C_9 and C_{10}, as well as $C_S^{(\prime)}$ and $C_P^{(\prime)}$. In comparison to Fig. 4, we focus here on the contours corresponding to $B_s \to \mu e$ rather than $B \to K^{(*)}\mu e$. This choice is justified by the fact that $B_s \to \mu e$ places stronger constraints on $[C'_{\ell edq}]_{1223}$ and $[C_{\ell edq}]_{2132}$, as clearly evident from Fig. 3. Analyzing the contours associated with the current limits for all the three processes, we observe that the strongest constraint along the x axes comes from $B_s \to \mu e$; however, along the y axes it comes from $\mathrm{CR}(\mu \to e)$. Turning to future limits, the current limit of $B_s \to \mu e$ surpasses $\mathrm{CR}(\mu \to e)$ (phase I) along the x axes, while along the y axes, both $\mathrm{CR}(\mu \to e)$ (phase I) and $\mu \to eee$ exert strong constraints. The limit from $\mathrm{CR}(\mu \to e)$ (phase II), while being the most influential constraint in the top plot for both WCs, slightly lags behind the current limit of $B_s \to \mu e$ along the $[C_{\ell edq}]_{2132}$ direction in the bottom plot. We notice that the contours of $\mu \to eee$ have negligible effects along $[C'_{\ell edq}]_{1223}$, since the RGE effects of $[C'_{\ell edq}]_{1223}$ have a minimal impact on the WCs contributing to $\mu \to eee$. However, it does contribute to $\mathrm{CR}(\mu \to e)$

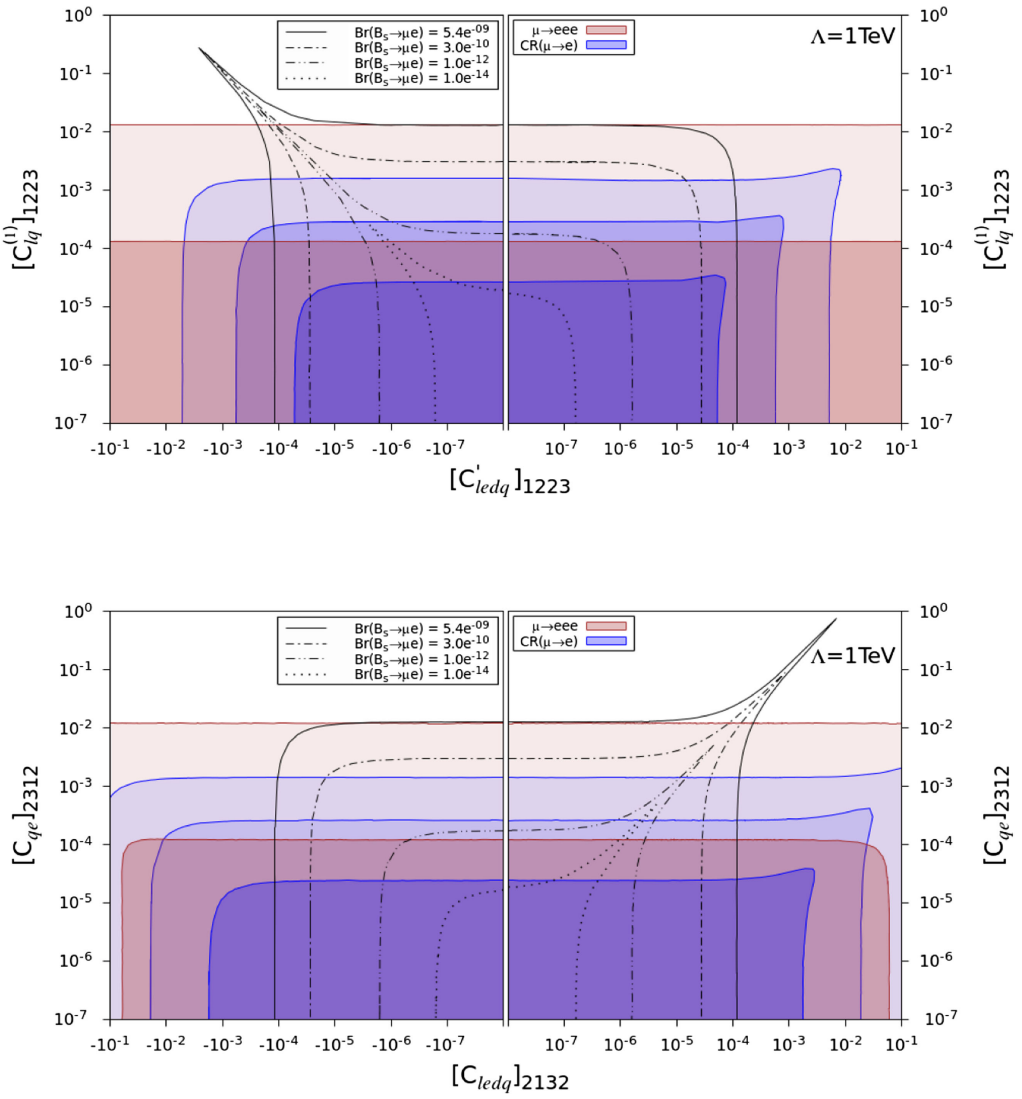

FIG. 5. With $\Lambda = 1$ TeV, contours of $B_s \to \mu e$ as a function of $[C_{\ell edq}]_{1223}$ and $[C^{(1)}_{\ell q}]_{1223}$. Color codes are the same as in Fig. 4.

through $[C_{\ell edq}]_{1222}$, as shown in Table IV. On the other hand, in the bottom plot, $[C_{\ell edq}]_{2132}$ mildly affects both $\mu \to eee$ and $\mathrm{CR}(\mu \to e)$ through dipole operators. Consequently, the current and future constraints on $\mu \to eee$ are notably weaker along the x axes when it comes to constraining both $[C'_{\ell edq}]_{1223}$ and $[C_{\ell edq}]_{2132}$. This trivial cancellation observed between the pair of WCs, in both the top and bottom figures, can be attributed to the cross terms appearing in Eq. (11). However, prominent cancellations are not observed in the other LFV processes, primarily due to the absence of cross terms between the corresponding WCs responsible for both $\mathrm{CR}(\mu \to e)$ and $\mu \to eee$ that are affected by the RGE flow.

Figure 6 displays the contours of $\mathcal{B}(B^0 \to K^{*0}\mu e)$, $\mu \to eee$ and $\mathrm{CR}(\mu \to e)$, in the plane of WCs $[C^{(1)}_{\phi\ell}]_{12}$ and $[C^{(1)}_{\ell q}]_{1223}$ (top) and $[C_{\phi e}]_{12}$ and $[C_{qe}]_{2312}$ (bottom), both considered at the energy scale $\Lambda = 1$ TeV. In this context, $[C^{(1)}_{\ell q}]_{1223}$ and $[C_{qe}]_{2312}$ pertain to LFVBDs, while $[C^{(1)}_{\phi\ell}]_{12}$ and $[C_{\phi e}]_{12}$ are relevant for $\mu \to eee$ and $\mathrm{CR}(\mu \to e)$. The color codes for the contours hold the same meaning as described in the previous paragraph. Looking into the current limits of the BRs, we find that the $\mathrm{CR}(\mu \to e)$ process imposes the strongest constraint along $[C^{(1)}_{\phi\ell}]_{12}$ (top) and $[C_{\phi e}]_{12}$ (bottom). However, along the y axes, the current limit of $\mathcal{B}(B^0 \to K^{*0}\mu e)$ surpasses the other LFV processes in constraining $[C^{(1)}_{\ell q}]_{1223}$ (top) and $[C_{qe}]_{2312}$ (bottom), respectively. Furthermore, considering future bounds we find that the contours of $\mu \to eee$ and $\mathrm{CR}(\mu \to e)$ (phase I) strongly constrain the WCs along x as well as y axes in both the plots. These future bounds from both the LFV processes closely coincide with the current bound of $\mathcal{B}(B^0 \to K^{*0}\mu e)$, especially in constraining $[C^{(1)}_{\ell q}]_{1223}$ (top) and $[C_{qe}]_{2312}$ (bottom).

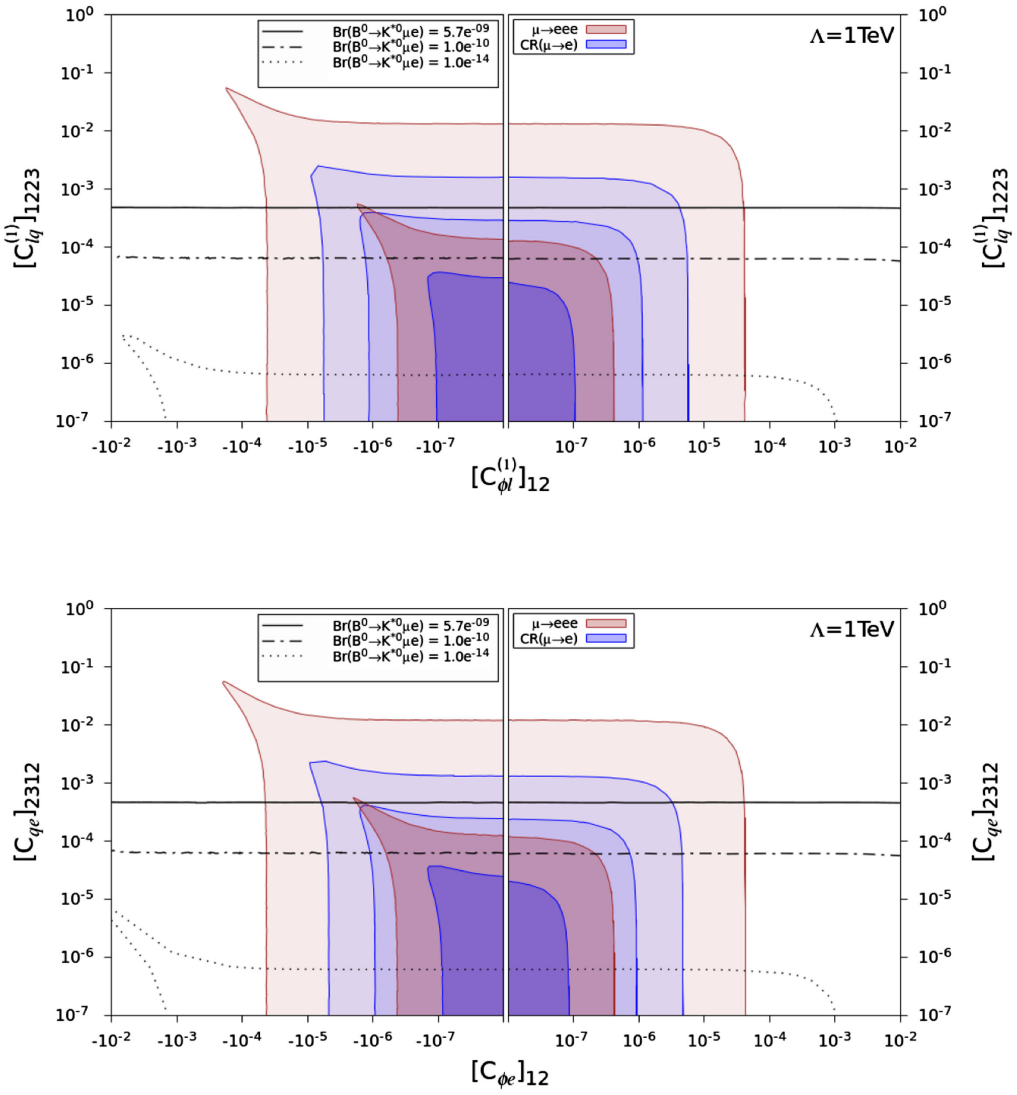

FIG. 6. With $\Lambda = 1$ TeV, contours of $B^0 \to K^{0*}\mu e$ as a function of $[C_{\phi\ell}^{(1)}]_{12}$ and $[C_{\ell q}^{(1)}]_{1223}$ (top) and $[C_{\phi e}]_{12}$ and $[C_{qe}]_{2312}$ (bottom). Color codes are the same as in Fig. 4.

Moreover, the future limit of CR($\mu \to e$) (phase II), although it imposes strong constraints on $[C_{\phi\ell}^{(1)}]_{12}$ (top) and $[C_{\phi e}]_{12}$ (bottom), is less efficient in constraining both $[C_{\ell q}^{(1)}]_{1223}$ (top) and $[C_{qe}]_{2312}$ (bottom). We note that, in regard to CR($\mu \to e$) and $\mu \to eee$, the observed pattern of cancellations between pairs of WCs in the top figure can again be understood from Eq. (49). The large contributions to both Higgs-lepton operators in Fig. 6 coming from $2q2\ell$ operators completely explains why $\mu \to eee$ and CR($\mu \to e$) processes dominate in constraining these operators. On the contrary, for the $2q2\ell$ operators, strong constraints mainly arise from LFVBDs. In regard to the bottom figure, a similar equation relating $[C_{\varphi e}]_{12}$ and $[C_{qe}]_{2312}$ can be found from corresponding RGEs to explain their behavior seen in the plot.

V. CONCLUSION

Using a model-independent framework of SMEFT, we analyzed how the limits from leptonic and semileptonic LFV B decay processes such as $B_s \to \mu^+ e^-, B^+ \to K^+\mu^+ e^-, B^0 \to K^{*0}\mu^+ e^-, B_s \to \phi\mu^- e^+$ may constrain relevant Wilson coefficients associated with dimension-six operators as mentioned in Table II. We use the usual match and run procedure where a SMEFT journey of appropriate Wilson coefficients from a high scale (Λ) to the electroweak scale would determine the starting of the evolution for the LEFT operators. The latter are then evolved down to a low scale like the mass scale m_b used to obtain the appropriate branching ratios. Apart from the said LFVBD limits, we also take into account how the bounds from LFV processes like CR($\mu \to e$), $\ell_i \to \ell_j\gamma$, $\ell_i \to \ell_j\ell_k\ell_m$, and $Z \to \ell_i\ell_j$, collectively referred as the other LFV

processes, are able to constrain the WCs. We used present BRs as well as some expected future limits as given in Table I while probing the WCs of importance and studied the interplay of the LFVBD and the other LFV processes. While direct effects from LFVBDs principally affect the associated WCs, the same set of the coefficients may receive constraints from the other LFV processes, too. Accordingly, the running effects and RGE mixing of different WCs can be quite important while we do a combined analysis of all these LFV processes. For each of the relevant SMEFT operators, we identify a few WCs that are heavily influenced because of RGE mixing and running and are, in turn, able to affect the different LFV processes considered in this analysis. In addition to studying the direct effects of LFVBD limits on the primarily important WCs, we also take into account how the same are affected indirectly via BR limits from the other LFV processes. The latter set of LFV limits, on the other hand, may provide estimates for the maximum levels of the LFVBDs that may duly be probed. Additionally, apart from considering prospective limits from Table I, we also considered two assumed levels of more stringent LFVBD limits simply to explore the potential of the interplay of all the LFV processes under discussion. We divide our analysis into two principal parts, namely, studying only one or two operators at a time. In the first part, the single operator analysis identifies the WCs that are maximally affected via RGE mixing and running effects for a given SMEFT scale ($\Lambda = 1$ TeV). We further estimated maximum possible values of Λ as obtained from a given LFV limit while assuming the concerned WC to be unity.

In regard to the RGE effects of LFVBD operators, it turns out that only $\mathcal{O}_{\varphi\ell}^{(1,3)}$ and $\mathcal{O}_{\varphi e}$, which affect most of the other LFV processes, receive significant impacts from $\mathcal{O}_{\ell q}^{(1,3)}$ and $\mathcal{O}_{qe}$. This correlation is shown in Table IV. For $\mathcal{O}_{ledq}$, the prominent RGE effect of $[C_{ledq}]_{1223}$ arises from the same WC with different quark index, namely, $[C_{ledq}]_{1222}$. Out of the six operators primarily associated with LFVBDs as shown in Table II, one finds from the 1D analysis (performed with $\Lambda = 1$ TeV) that only the operators with left-handed quark currents, such as $C_{\ell q}^{(1,3)}$ and C_{qe}, are able to contribute to the other LFV processes significantly (Fig. 2). In contrast, the operators with right-handed quark currents, namely, $C_{\ell d}$ and C_{ed} that contribute to $C'_{(9,10)}$, are relevant only for LFVBDs, with hardly having any effect on the other LFV processes.

The later part of the 1D analysis for the LFV operators that probed the scale Λ while considering the current and future experimental bounds results in Fig. 2. The major takeaway from this energy analysis is that, in the $e-\mu$ sector, current sensitivities (blue bars) of BRs of LFVBDs coming from operators $\mathcal{O}_{\ell q}^{(1,3)}, \mathcal{O}_{qe}$, and $\mathcal{O}_{ledq}$, are competitive compared to other similar low-energy observables, especially with $\mathrm{CR}(\mu \to e)$ or sometimes with $\mu \to e\gamma$. The result remains the same if we consider future (green shades) or assumed enhancement of sensitivities (darker and lighter red shades). Therefore, if new physics primarily generates the LFVBD operators between the scales $\Lambda = 100$ and 1000 TeV, we expect $B^0 \to K^{*0}\mu^+e^-$, $B^+ \to K^+\mu^+e^-$, $B_s \to \phi\mu^-e^+$, $B_s \to \mu^+e^-$, and $\mathrm{CR}(\mu \to e)$ to be quite promising in regard to future experiments.

In this sector, two processes, namely, $\mu \to eee$ and $\mathrm{CR}(\mu \to e)$, can put indirect constraints on BRs of several B-decay processes as shown in Table VI. From this analysis, we find that for the processes $B^+ \to K^+\mu^+e^-, B \to K^*\mu^+e^-$, and $B_s \to \phi\mu^-e^+$, the BRs $\sim 10^{-10}$ which is just 1 order of magnitude below the current LHCb bounds and within the anticipated future limit proposed by LHCb-II. On the other hand, the $\ell - \tau$ sector is more promising, as they can be probed at much lower energy, clearly seen from the plots of Fig. 3.

In the 2D case, we consider two nonvanishing operators at a time for a fixed value of $\Lambda = 1$ TeV. Both WCs may directly be related to LFVBDs (Figs. 4 and 5) or one related to LFVBD and another corresponding to a different LFV process other than any of the LFVBDs (Fig. 6). We begin with considering a pair of WCs responsible for LFVBDs only. Figure 4 shows a plot for the WCs in the plane of $C_{\ell q}^{(1)}$ and $C_{\ell q}^{(3)}$, where present and future BRs of LFV processes like $B \to K^*\mu^+e^-$, $\mathrm{CR}(\mu \to e)$, and $\mu \to eee$ are used for the contours. Following the current limits we find that, although $B \to K^*\mu^+e^-$ imposes the strongest constraints on these two WCs, future predictions for $\mu \to eee$ and phase I of $\mathrm{CR}(\mu \to e)$ overcome these limits. To be specific, the new parameter space constrained by $\mu \to eee$ for this set of WCs reduces the $\mathcal{B}(B \to K^*\mu e)$ by 1 order of magnitude from the existing bound that can potentially be probed by Belle II and LHCb experiments. Similarly, in Fig. 5 we show the contours for $B_s \to \mu^+e^-$, $\mathrm{CR}(\mu \to e)$, and $\mu \to eee$ in the plane of $[C_{\ell edq}]_{1223}$ vs $[C_{\ell q}^{(1)}]_{1223}$ and $[C_{\ell edq}]_{2132}$ vs $[C_{qe}]_{2312}$. The figures show that RGE running of $[C_{\ell edq}]_{1223}$ has very little impact on the WCs contributing to $\mu \to eee$, whereas its influence on $\mathrm{CR}(\mu \to e)$ via $[C_{\ell edq}]_{1222}$ is relatively more significant. This is consistent with the result shown in Table IV. Moreover, it turns out that $[C_{\ell edq}]_{2132}$ has mild influence on both $\mu \to eee$ and $\mathrm{CR}(\mu \to e)$ through dipole operators.

In further study of our 2D analysis, we picked up a pair of operators, of which one is exclusively responsible for LFVBDs and the other one is significant for several other LFV processes. From Fig. 6 we find that, while constraining $[C_{\ell q}^{(1)}]_{1223}$ and $[C_{qe}]_{2312}$, future bounds from $\mu \to eee$ and $\mathrm{CR}(\mu \to e)$ (phase I) closely coincide with the current bound of $\mathcal{B}(B^0 \to K^{*0}\mu e)$. This implies that different LFVBD processes are competitive in order to impose constraints on the $2q2\ell$ operators. On the other hand, Higgs-lepton

operators get the strongest constraints from other LFV processes only. The flat directions in these plots are indicative of the nontrivial RGE effects between the respective pair of operators.

ACKNOWLEDGMENTS

We have been benefited from discussion with X. Marcano. I. A. would like to thank the Council of Scientific and Industrial Research (File No. 09/080(1111)/2019-EMR-I), India for financial support.

APPENDIX: LEPTON FLAVOR VIOLATING Z BOSON DECAYS ($Z \to \ell_i \ell_j$)

The effective interactions involving the Z boson and the SM leptons, including those responsible for LFV effects, are given by the following Lagrangian [131]:

$$\mathcal{L}^{Z}_{\text{eff}} = \left[\left(g_{VR}\delta_{ij} + \delta g^{ij}_{VR}\right)\overline{\ell}_i \gamma^\mu P_R \ell_j + \left(g_{VL}\delta_{ij} + \delta g^{ij}_{VL}\right)\overline{\ell}_i \gamma^\mu P_L \ell_j\right] Z_\mu + \left[\delta g^{ij}_{TR}\overline{\ell}_i \sigma^{\mu\nu} P_R \ell_j + g^{ij}_{TL}\overline{\ell}_i \sigma^{\mu\nu} P_L \ell_j\right] Z_{\mu\nu} + \text{H.c.}, \tag{A1}$$

where

$$g_{VR} = \frac{e s_{\text{w}}}{c_{\text{w}}}, \qquad g_{VL} = \frac{e}{s_{\text{w}} c_{\text{w}}}\left(-\frac{1}{2} + s^2_{\text{w}}\right) \tag{A2}$$

are the SM couplings of the Z to, respectively, right- and left-handed lepton currents, with s_{w} (c_{w}) being the sine (cosine) of the weak mixing angle. New physics effects are encoded in the effective couplings $\delta g_{V/T}$, which at the tree level match the SMEFT operators as follows:

$$\delta g^{ij}_{VR} = -\frac{e v^2}{2 s_{\text{w}} c_{\text{w}} \Lambda^2} C^{ij}_{\varphi e}, \qquad \delta g^{ij}_{VL} = -\frac{e v^2}{2 s_{\text{w}} c_{\text{w}} \Lambda^2}\left(C^{(1)ij}_{\varphi \ell} + C^{(3)ij}_{\varphi \ell}\right), \tag{A3}$$

$$\delta g^{ij}_{TR} = \delta g^{ji}_{TL} = -\frac{v}{\sqrt{2}\Lambda^2}\left(s_{\text{w}} C^{ij}_{eB} + c_{\text{w}} C^{ij}_{eW}\right), \tag{A4}$$

where the WCs have to be evaluated at the scale $\mu = m_Z$.

The branching ratios of the Z decays into leptons, in particular, of the LFV modes, are then given by the following expression [111,131]:

$$\text{BR}(Z \to \ell_i \ell_j) = \frac{m_Z}{12\pi\Gamma_Z}\left(\left|g_{VR}\delta_{ij} + \delta g^{ij}_{VR}\right|^2 + \left|g_{VL}\delta_{ij} + \delta g^{ij}_{VL}\right|^2 + \frac{m^2_Z}{2}\left|\delta g^{ij}_{TR}\right|^2 + \frac{m^2_Z}{2}\left|\delta g^{ij}_{TL}\right|^2\right), \tag{A5}$$

where $\Gamma_Z = 2.4952(23)$ GeV is the total decay width of the Z boson, and we summed over the two possible combinations of lepton charges, $\ell^{\pm}_i \ell^{\mp}_j$.

[1] M. E. Peskin and D. V. Schroeder, *An Introduction to Quantum Field Theory* (Addison-Wesley, Reading, MA, 1995).
[2] S. Myers and E. Picasso, The design, construction and commissioning of the CERN large electron positron collider, Contemp. Phys. **31**, 387 (1990).
[3] R. R. Wilson, The Tevatron, Phys. Today **30**, 23 (1977).
[4] L. Evans and P. Bryant, LHC machine, J. Instrum. **3**, S08001 (2008).
[5] G. Aad *et al.*, Observation of a new particle in the search for the Standard Model Higgs boson with the ATLAS detector at the LHC, Phys. Lett. B **716**, 1 (2012).
[6] A. Crivellin and B. Mellado, Anomalies in particle physics, arXiv:2309.03870.
[7] Y. Fukuda *et al.*, Evidence for oscillation of atmospheric neutrinos, Phys. Rev. Lett. **81**, 1562 (1998).
[8] Q. R. Ahmad *et al.*, Direct evidence for neutrino flavor transformation from neutral current interactions in the Sudbury Neutrino Observatory, Phys. Rev. Lett. **89**, 011 (2002).
[9] L. Calibbi and G. Signorelli, Charged lepton flavour violation: An experimental and theoretical introduction, Riv. Nuovo Cimento **41**, 71 (2018).

[10] M. Ardu and G. Pezzullo, Introduction to charged lepton flavor violation, Universe **8**, 299 (2022).

[11] E. P. Hincks and B. Pontecorvo, Search for gamma-radiation in the 2.2-microsecond meson decay process, Phys. Rev. **73**, 257 (1948).

[12] A. M. Baldini *et al.*, Search for the lepton flavour violating decay $\mu^+ \to e^+\gamma$ with the full dataset of the MEG experiment, Eur. Phys. J. C **76**, 434 (2016).

[13] A. M. Baldini *et al.*, The design of the MEG II experiment, Eur. Phys. J. C **78**, 380 (2018).

[14] U. Bellgardt *et al.*, Search for the decay $\mu^+ \to e^+e^+e^-$, Nucl. Phys. **B299**, 1 (1988).

[15] W. H. Bertl *et al.*, A search for muon to electron conversion in muonic gold, Eur. Phys. J. C **47**, 337 (2006).

[16] F. Wauters, The Mu3e experiment, SciPost Phys. Proc. **5**, 020 (2021).

[17] L. Bartoszek *et al.*, Mu2e technical design report, arXiv:1501.05241.

[18] R. Abramishvili *et al.*, COMET phase-I technical design report, Prog. Theor. Exp. Phys. **2020**, 033C01 (2020).

[19] H. Natori, DeeMe experiment—An experimental search for a mu-e conversion reaction at J-PARC MLF, Nucl. Phys. B, Proc. Suppl. **248–250**, 52 (2014).

[20] B. Aubert *et al.*, The *BABAR* detector, Nucl. Instrum. Methods Phys. Res., Sect. A **479**, 1 (2002).

[21] A. Abashian *et al.*, The Belle detector, Nucl. Instrum. Methods Phys. Res., Sect. A **479**, 117 (2002).

[22] B. Aubert *et al.*, Searches for lepton flavor violation in the decays $\tau^\pm \to e^\pm\gamma$ and $\tau^\pm \to \mu^\pm\gamma$, Phys. Rev. Lett. **104**, 021 (2010).

[23] A. Abdesselam *et al.*, Search for lepton-flavor-violating tau-lepton decays to $\ell\gamma$ at Belle, J. High Energy Phys. 10 (2021) 019.

[24] W. Altmannshofer *et al.*, The Belle II physics book, Prog. Theor. Exp. Phys. **2019**, 123C01 (2019); **2020**, 029201(E) (2020).

[25] R. Aaij *et al.*, Search for the lepton flavour violating decay $\tau^{--} \to \mu^{--}\mu^+\mu^{--}$, J. High Energy Phys. 02 (2015) 121.

[26] G. Aad *et al.*, Search for lepton-flavor-violation in Z-boson decays with τ leptons with the ATLAS detector, Phys. Rev. Lett. **127**, 271 (2022).

[27] G. Aad *et al.*, Search for the charged-lepton-flavor-violating decay $Z \to e\mu$ in pp collisions at $\sqrt{s} = 13$ TeV with the ATLAS detector, Phys. Rev. D **108**, 032 (2023).

[28] G. Aad *et al.*, Search for lepton-flavor violating decays of the Higgs boson in $\sqrt{s} = 13$ TeV pp collisions with the ATLAS detector, Phys. Lett. B **800**, 135 (2020).

[29] A. M. Sirunyan *et al.*, Search for lepton-flavor violating decays of the Higgs boson in the $\mu\tau$ and $e\tau$ final states in proton-proton collisions at $\sqrt{s} = 13$ TeV, Phys. Rev. D **104**, 032 (2021).

[30] W. Altmannshofer, C. Caillol, M. Dam, S. Xella, and Y. Zhang, Charged lepton flavour violation in heavy particle decays, arXiv:2205.10576.

[31] R. Aaij *et al.*, Search for the lepton-flavour violating decays $B^0_{(s)} \to e^\pm\mu^\mp$, J. High Energy Phys. 03 (2018) 078.

[32] R. Aaij *et al.*, Search for the lepton-flavor-violating decays $B^0_s \to \tau^\pm\mu^\mp$ and $B^0 \to \tau^\pm\mu^\mp$, Phys. Rev. Lett. **123**, 211 (2019).

[33] R. Aaij *et al.*, Search for lepton-flavor violating decays $B^+ \to K^+\mu^\pm e^\mp$, Phys. Rev. Lett. **123**, 241 (2019).

[34] R. Aaij *et al.* (LHCb Collaboration), Search for the lepton-flavour violating decays $B^0 \to K^{*0}\mu^\pm e^\mp$ and $B^0_s \to \phi\mu^\pm e^\mp$, J. High Energy Phys. 06 (2023) 073.

[35] R. Aaij *et al.*, Physics case for an LHCb Upgrade II—Opportunities in flavour physics, and beyond, in the HL-LHC era, arXiv:1808.08865.

[36] LHCb collaboration, Future physics potential of LHCb (2022), https://cds.cern.ch/record/2806113/files/LHCb-PUB-2022-012.pdf.

[37] A. Blondel *et al.*, Research proposal for an experiment to search for the decay $\mu \to eee$, arXiv:1301.6113.

[38] Y. Kuno, A search for muon-to-electron conversion at J-PARC: The COMET experiment, Prog. Theor. Exp. Phys. **2013**, 022C01 (2013).

[39] K. Hayasaka *et al.*, Search for lepton flavor violating τ decays into three leptons with 719 million produced $\tau^+\tau^-$ pairs, Phys. Lett. B **687**, 139 (2010).

[40] Y. Miyazaki *et al.*, Search for lepton flavor violating τ decays into three leptons with 719 million produced $\tau^+\tau^-$ pairs, Phys. Lett. B **648**, 341 (2007).

[41] B. Aubert *et al.*, Search for lepton flavor violating decays $\tau^\pm \to \ell^\pm\pi^0$, $\ell^\pm\eta$, $\ell^\pm\eta'$, Phys. Rev. Lett. **98**, 061 (2007).

[42] Y. Miyazaki *et al.*, Search for lepton-flavor-violating tau decays into a lepton and a vector meson, Phys. Lett. B **699**, 251 (2011).

[43] R. Akers *et al.*, A search for lepton flavor violating Z0 decays, Z. Phys. C **67**, 555 (1995).

[44] G. Aad *et al.*, Search for the lepton flavor violating decay $Z \to e\mu$ in pp collisions at $\sqrt{s}$ TeV with the ATLAS detector, Phys. Rev. D **90**, 072 (2014).

[45] The CEPC Study Group, CEPC Conceptual Design Report: Volume 2–Physics & Detector, arXiv:1811.10545.

[46] The CEPC Study Group, CEPC Conceptual Design Report: Volume 1–Accelerator, arXiv:1809.00285.

[47] M. Benedikt *et al.*, Future Circular Collider–European Strategy Update Documents, CERN Report No. CERN-ACC-2019-0007, 2019.

[48] G. Hernández-Tomé, J. I. Illana, M. Masip, G. López Castro, and P. Roig, Effects of heavy Majorana neutrinos on lepton flavor violating processes, Phys. Rev. D **101**, 075020 (2020).

[49] G. Aad *et al.*, Search for charged-lepton-flavour violation in Z-boson decays with the ATLAS detector, Nat. Phys. **17**, 819 (2021).

[50] P. Abreu *et al.*, Search for lepton flavor number violating Z0 decays, Z. Phys. C **73**, 243 (1997).

[51] S. Watanuki *et al.*, Search for the lepton flavour violating decay $B^+ \to K^+\mu^-\tau^+$ using B^{*0}_{s2} decays, J. High Energy Phys. 06 (2020) 129.

[52] LHCb Collaboration, Search for the lepton-flavour violating decays $B^0 \to K^{*0}\tau^\pm\mu^\mp$, J. High Energy Phys. 06 (2023) 143.

[53] S. Davidson, $\mu \to e\gamma$ in the 2HDM: An exercise in EFT, Eur. Phys. J. C **76**, 258 (2016).

[54] R. Diaz, R. Martinez, and J. A. Rodriguez, Lepton flavor violation in the two Higgs doublet model type III, Phys. Rev. D **63**, 095 (2001).

[55] R. A. Diaz, R. Martinez, and J. A. Rodriguez, Phenomenology of lepton flavor violation in 2HDM(3) from $(g-2)_\mu$ and leptonic decays, Phys. Rev. D **67**, 075 (2003).

[56] D. Chang, W. S. Hou, and W.-Y. Keung, Two loop contributions of flavor changing neutral Higgs bosons to $\mu \to e\gamma$, Phys. Rev. D **48**, 217 (1993).

[57] P. Paradisi, Higgs-mediated $e \to \mu$ transitions in II Higgs doublet model and supersymmetry, J. High Energy Phys. 08 (2006) 047.

[58] R. Barbieri, L. J. Hall, and A. Strumia, Violations of lepton flavor and CP in supersymmetric unified theories, Nucl. Phys. **B445**, 219 (1995).

[59] J. Hisano, T. Moroi, K. Tobe, and M. Yamaguchi, Lepton flavor violation via right-handed neutrino Yukawa couplings in supersymmetric standard model, Phys. Rev. D **53**, 2442 (1996).

[60] J. Hisano, T. Moroi, K. Tobe, and M. Yamaguchi, Exact event rates of lepton flavor violating processes in supersymmetric SU(5) model, Phys. Lett. B **391**, 341 (1997); **397**, 357(E) (1997).

[61] J. Hisano and D. Nomura, Solar and atmospheric neutrino oscillations and lepton flavor violation in supersymmetric models with the right-handed neutrinos, Phys. Rev. D **59**, 116 (1999).

[62] J. R. Ellis, M. E. Gomez, G. K. Leontaris, S. Lola, and D. V. Nanopoulos, Charged lepton flavor violation in the light of the Super-Kamiokande data, Eur. Phys. J. C **14**, 319 (2000).

[63] J. A. Casas and A. Ibarra, Oscillating neutrinos and $\mu \to e, \gamma$, Nucl. Phys. **B618**, 171 (2001).

[64] L. Calibbi, A. Faccia, A. Masiero, and S. K. Vempati, Lepton flavour violation from SUSY-GUTs: Where do we stand for MEG, PRISM/PRIME and a super flavour factory, Phys. Rev. D **74**, 116 (2006).

[65] L. Calibbi, D. Chowdhury, A. Masiero, K. M. Patel, and S. K. Vempati, Status of supersymmetric type-I seesaw in SO(10) inspired models, J. High Energy Phys. 11 (2012) 040.

[66] M. Hirsch, F. R. Joaquim, and A. Vicente, Constrained SUSY seesaws with a 125 GeV Higgs, J. High Energy Phys. 11 (2012) 105.

[67] L. Calibbi, I. Galon, A. Masiero, P. Paradisi, and Y. Shadmi, Charged slepton flavor post the 8 TeV LHC: A simplified model analysis of low-energy constraints and LHC SUSY searches, J. High Energy Phys. 10 (2015) 043.

[68] J. L. Evans, K. Kadota, and T. Kuwahara, Revisiting flavor and CP violation in supersymmetric SU(5) with right-handed neutrinos, Phys. Rev. D **98**, 075 (2018).

[69] K. Hirao and T. Moroi, Leptonic CP and flavor violations in SUSY GUT with right-handed neutrinos, Phys. Rev. D **104**, 035 (2021).

[70] U. Chattopadhyay, D. Das, and S. Mukherjee, Probing lepton flavor violating decays in MSSM with non-holomorphic soft terms, J. High Energy Phys. 06 (2020) 015.

[71] J. Girrbach, S. Mertens, U. Nierste, and S. Wiesenfeldt, Lepton flavour violation in the MSSM, J. High Energy Phys. 05 (2010) 026.

[72] I. Masina and C. A. Savoy, Sleptonarium: Constraints on the CP and flavor pattern of scalar lepton masses, Nucl. Phys. **B661**, 365 (2003).

[73] T. Goto, Y. Okada, T. Shindou, M. Tanaka, and R. Watanabe, Lepton flavor violation in the supersymmetric seesaw model after the LHC 8 TeV run, Phys. Rev. D **91**, 033 (2015).

[74] A. Vicente, Lepton flavor violation beyond the MSSM, Adv. High Energy Phys. **2015**, 686 (2015).

[75] C. Bonilla, M. E. Krauss, T. Opferkuch, and W. Porod, Perspectives for detecting lepton flavour violation in left-right symmetric models, J. High Energy Phys. 03 (2017) 027.

[76] W. Altmannshofer, S. Gori, M. Pospelov, and I. Yavin, Quark flavor transitions in $L_\mu - L_\tau$ models, Phys. Rev. D **89**, 095 (2014).

[77] S. L. Glashow, D. Guadagnoli, and K. Lane, Lepton flavor violation in B decays?, Phys. Rev. Lett. **114**, 091 (2015).

[78] R. Alonso, B. Grinstein, and J. Martin Camalich, Lepton universality violation and lepton flavor conservation in B-meson decays, J. High Energy Phys. 10 (2015) 184.

[79] A. Greljo, G. Isidori, and D. Marzocca, On the breaking of lepton flavor universality in B decays, J. High Energy Phys. 07 (2015) 142.

[80] S. M. Boucenna, J. W. F. Valle, and A. Vicente, Are the B decay anomalies related to neutrino oscillations?, Phys. Lett. B **750**, 367 (2015).

[81] A. Falkowski, M. Nardecchia, and R. Ziegler, Lepton flavor non-universality in B-meson decays from a U(2) flavor model, J. High Energy Phys. 11 (2015) 173.

[82] D. Guadagnoli, D. Melikhov, and M. Reboud, More lepton flavor violating observables for LHCb's run 2, Phys. Lett. B **760**, 442 (2016).

[83] F. Feruglio, P. Paradisi, and A. Pattori, Revisiting lepton flavor universality in B decays, Phys. Rev. Lett. **118**, 011 (2017).

[84] I. de Medeiros Varzielas and G. Hiller, Clues for flavor from rare lepton and quark decays, J. High Energy Phys. 06 (2015) 072.

[85] S. Sahoo and R. Mohanta, Lepton flavor violating B meson decays via a scalar leptoquark, Phys. Rev. D **93**, 114 (2016).

[86] M. Duraisamy, S. Sahoo, and R. Mohanta, Rare semi-leptonic $B \to K(\pi) l_i^- l_j^+$ decay in a vector leptoquark model, Phys. Rev. D **95**, 035 (2017).

[87] D. Bečirević, N. Košnik, O. Sumensari, and R. Zukanovich Funchal, Palatable leptoquark scenarios for lepton flavor violation in exclusive $b \to s\ell_1\ell_2$ modes, J. High Energy Phys. 11 (2016) 035.

[88] A. Crivellin, D. Müller, A. Signer, and Y. Ulrich, Correlating lepton flavor universality violation in B decays with $\mu \to e\gamma$ using leptoquarks, Phys. Rev. D **97**, 015 (2018).

[89] J.-H. Sheng, R.-M. Wang, and Y.-D. Yang, Scalar leptoquark effects in the lepton flavor violating exclusive $b \to s\ell_i^-\ell_j^+$ decays, Int. J. Theor. Phys. **58**, 480 (2019).

[90] S. Kumbhakar, R. Sain, and J. Vardani, Lepton flavor violating decays, J. Phys. G **50**, 095 (2023).

[91] A. Crivellin, B decays and lepton flavour (universality) violation, Nuovo Cimento Soc. Ital. Fis. **38C**, 134 (2016).

[92] A. Crivellin, L. Hofer, J. Matias, U. Nierste, S. Pokorski, and J. Rosiek, Lepton-flavour violating B decays in generic Z' models, Phys. Rev. D **92**, 054 (2015).

[93] D. Bečirević, O. Sumensari, and R. Zukanovich Funchal, Lepton flavor violation in exclusive $b \to s$ decays, Eur. Phys. J. C **76**, 134 (2016).

[94] Fayyazuddin, M. J. Aslam, and C.-D. Lu, Lepton flavor violating decays of B and K mesons in models with extended gauge group, Int. J. Mod. Phys. A **33**, 850 (2018).

[95] J.-H. Sheng, J.-J. Song, R.-M. Wang, and Y.-D. Yang, The lepton flavor violating exclusive $\bar{b} \to \bar{s}\ell_i^-\ell_j^+$ decays in SUSY without R-parity, Nucl. Phys. **B930**, 69 (2018).

[96] H. Georgi, Effective field theory, Annu. Rev. Nucl. Part. Sci. **43**, 209 (1993).

[97] W. Buchmuller and D. Wyler, Effective Lagrangian analysis of new interactions and flavor conservation, Nucl. Phys. **B268**, 621 (1986).

[98] D. B. Kaplan, Lectures on effective field theory, https://archive.int.washington.edu/users/dbkaplan/572_16/EFT.pdf.

[99] P. Bechtle, C. Chall, M. King, M. Kraemer, P. Maettig, and M. Stöltzner, Bottoms up: Standard model effective field theory from a model perspective, arXiv:2201.08819.

[100] B. Grzadkowski, M. Iskrzynski, M. Misiak, and J. Rosiek, Dimension-six terms in the standard model Lagrangian, J. High Energy Phys. 10 (2010) 085.

[101] S. Davidson, Y. Kuno, and M. Yamanaka, Selecting $\mu \to e$ conversion targets to distinguish lepton flavour-changing operators, Phys. Lett. B **790**, 380 (2019).

[102] A. Crivellin, S. Davidson, G. M. Pruna, and A. Signer, Renormalisation-group improved analysis of $\mu \to e$ processes in a systematic effective-field-theory approach, J. High Energy Phys. 05 (2017) 117.

[103] V. Cirigliano, S. Davidson, and Y. Kuno, Spin-dependent $\mu \to e$ conversion, Phys. Lett. B **771**, 242 (2017).

[104] S. Davidson, Y. Kuno, and A. Saporta, Spin-dependent $\mu \to e$ conversion on light nuclei, Eur. Phys. J. C **78**, 109 (2018).

[105] S. Davidson, Y. Kuno, Y. Uesaka, and M. Yamanaka, Probing $\mu e\gamma\gamma$ contact interactions with $\mu \to e$ conversion, Phys. Rev. D **102**, 115 (2020).

[106] S. Davidson, Completeness and complementarity for $\mu \to e\gamma\mu \to e\bar{e}e$ and $\mu A \to eA$, J. High Energy Phys. 02 (2021) 172.

[107] V. Cirigliano, K. Fuyuto, C. Lee, E. Mereghetti, and B. Yan, Charged lepton flavor violation at the EIC, J. High Energy Phys. 03 (2021) 256.

[108] J. Kumar, Renormalization group improved implications of semileptonic operators in SMEFT, J. High Energy Phys. 01 (2022) 107.

[109] L. Calibbi, A. Crivellin, and T. Ota, Effective field theory approach to $b \to s\ell\ell^{(\prime)}$, $B \to K^{(*)}\nu\bar{\nu}$ and $B \to D^{(*)}\tau\nu$ with third generation couplings, Phys. Rev. Lett. **115**, 181 (2015).

[110] S. Descotes-Genon, D. A. Faroughy, I. Plakias, and O. Sumensari, Probing lepton flavor violation in meson decays with LHC data, Eur. Phys. J. C **83**, 753 (2023).

[111] A. Crivellin, S. Najjari, and J. Rosiek, Lepton flavor violation in the standard model with general dimension-six operators, J. High Energy Phys. 04 (2014) 167.

[112] G. M. Pruna and A. Signer, The $\mu \to e\gamma$ decay in a systematic effective field theory approach with dimension 6 operators, J. High Energy Phys. 10 (2014) 014.

[113] R. Alonso, B. Grinstein, and J. Martin Camalich, $SU(2) \times U(1)$ gauge invariance and the shape of new physics in rare B decays, Phys. Rev. Lett. **113**, 241 (2014).

[114] J. Aebischer, A. Crivellin, M. Fael, and C. Greub, Matching of gauge invariant dimension-six operators for $b \to s$ and $b \to c$ transitions, J. High Energy Phys. 05 (2016) 037.

[115] L. Calibbi, X. Marcano, and J. Roy, Z lepton flavour violation as a probe for new physics at future e^+e^- colliders, Eur. Phys. J. C **81**, 1054 (2021).

[116] J. M. Cullen and B. D. Pecjak, Higgs decay to fermion pairs at NLO in SMEFT, J. High Energy Phys. 11 (2020) 079.

[117] L. Calibbi, T. Li, X. Marcano, and M. A. Schmidt, Indirect constraints on lepton-flavor-violating quarkonium decays, Phys. Rev. D **106**, 115 (2022).

[118] E. E. Jenkins, A. V. Manohar, and M. Trott, Renormalization group evolution of the standard model dimension six operators I: Formalism and λ dependence, J. High Energy Phys. 10 (2013) 087.

[119] E. E. Jenkins, A. V. Manohar, and M. Trott, Renormalization group evolution of the standard model dimension six operators II: Yukawa dependence, J. High Energy Phys. 01 (2014) 035.

[120] R. Alonso, E. E. Jenkins, A. V. Manohar, and M. Trott, Renormalization group evolution of the standard model dimension six operators III: Gauge coupling dependence and phenomenology, J. High Energy Phys. 04 (2014) 159.

[121] B. Grinstein, M. J. Savage, and M. B. Wise, $B \to X_s e^+e^-$ in the six quark model, Nucl. Phys. **B319**, 271 (1989).

[122] E. E. Jenkins, A. V. Manohar, and P. Stoffer, Low-energy effective field theory below the electroweak scale: Operators and matching, J. High Energy Phys. 03 (2018) 016.

[123] E. E. Jenkins, A. V. Manohar, and P. Stoffer, Low-energy effective field theory below the electroweak scale: Anomalous dimensions, J. High Energy Phys. 01 (2018) 084.

[124] J. Aebischer, J. Kumar, and D. M. Straub, WILSON: A PYTHON package for the running and matching of Wilson coefficients above and below the electroweak scale, Eur. Phys. J. C **78**, 1026 (2018).

[125] D. M. Straub, FLAVIO: A PYTHON package for flavour and precision phenomenology in the standard model and beyond, arXiv:1810.08132.

[126] G. Buchalla, A. J. Buras, and M. E. Lautenbacher, Weak decays beyond leading logarithms, Rev. Mod. Phys. **68**, 1125 (1996).

[127] C. Bobeth, G. Hiller, and G. Piranishvili, Angular distributions of $\bar{B} \to \bar{K}\ell^+\ell^-$ decays, J. High Energy Phys. 12 (2007) 040.

[128] Y. Kuno and Y. Okada, Muon decay and physics beyond the standard model, Rev. Mod. Phys. **73**, 151 (2001).

[129] R. Kitano, M. Koike, and Y. Okada, Detailed calculation of lepton flavor violating muon electron conversion rate for various nuclei, Phys. Rev. D **66**, 096 (2002); **76**, 059902(E) (2007).

[130] M. Hernández Villanueva, Experimental review of lepton flavor violation searches, in *Proceedings of the 20th Conference on Flavor Physics and CP Violation* (2022), arXiv:2208.02723.

[131] A. Brignole and A. Rossi, Anatomy and phenomenology of $\mu - \tau$ lepton flavor violation in the MSSM, Nucl. Phys. **B701**, 3 (2004).